이학석사 학위논문

Sedimentary Processes and Depositional Environments of the Sesong Formation (Miaolingian-Furongian), Taebaeksan Basin

태백산 분지 세송층의 퇴적과정과 퇴적환경

2023년 8월

서울대학교 대학원

지구환경과학부

김 소 정

Sedimentary Processes and Depositional Environments of the Sesong Formation (Miaolingian-Furongian), Taebaeksan Basin

지도 교수 우 주 선

이 논문을 이학석사 학위논문으로 제출함

2023년 5월

서울대학교 대학원

지구환경과학부

김 소 정

김소정의 이학석사 학위논문을 인준함

2023년 7월

위 원 장 _____ (인)

부위원장 _____ (인)

위 원 _____ (인)

Abstract

Sedimentary Processes and Depositional Environments of the Sesong Formation (Miaolingian-Furongian), Taebaeksan Basin

This study mainly deals with sedimentary facies analysis and interpretation of depositional environments of the Sesong Formation (Miaolingian- Furongian), Taebaek Group, Taebaeksan Basin with emphasis on sandstone-prone upper part. The upper part of the Sesong Formation comprises eight sedimentary facies defined in drilled core and outcrop sections. Three facies associations (FAs) were designated from the assemblage of the sedimentary facies. FA1 exhibits bioturbated sandstone facies comprising predominantly medium to fine-grained sediment with a notable degree of bioturbation index (BI 3-5). Additionally, it displays distinct intercalations of the pack to grainstone facies. FA1 represents the most proximal portion of the offshore transition, the upper offshore transition. FA2 encompasses bioturbated sandstone facies characterized by a lower bioturbation index compared to FA1. Furthermore, FA2 exhibits a substantial increase in the amount of intercalated mudstone and limestone conglomerate facies compared to those in FA1. FA3 is dominated by fine-grained laminated sandstone and mudstone facies without bioturbation. FA 2 and FA3 represent the middle and lower offshore transition zones, respectively. The facies association changes upward from FA3 to FA1 in the lower part of the upper Sesong Formation and, in turn, changes back to FA3, suggesting progressive shallowing from an offshore environment to an offshore transition environment and following deepening. Elaborate analysis of sedimentary structure, grain size, and bioturbation index of the sandstone facies allowed the systematic subdivision of the offshore transition zone, which is

important in wave-dominated ramp-type platforms. A deformed limestone conglomerate beds overlain by dendrolite bioherms was newly discovered within the sandstone-dominated part of the formation. The deposition and deformation structures of the disorganized limestone conglomerate, sharp hardground surface, and dendrolite bioherms are interpreted as a slump deposit and microbial cover on top of it, intervened by a non-depositional period. The slumping and the non-deposition give rise to the possibility of the existence of relatively steep slope and laterally restricted sedimentary system. Integrating these evidences and sandstone dominant Sesong Formation in the middle of carbonate platform strata can be a suggestive of a delta system where delta front slope and delta lobe switching influenced the sedimentation rate of the Sesong Formation.

Keywords: Facies analysis, depositional environment, offshore transition, slumped bed, microbialite, calcified microbes, late Cambrian

***Student Number*:** 2021-28244

Contents

1. Introduction

The lower Paleozoic Joseon Supergroup in the Taebaeksan Basin is a well-known mixed siliciclastic-carbonate succession deposited in a shallow marine platform (Chough et al., 2000; Kwon et al., 2006). It consists of five lithologic units: Taebaek, Yeongwol, Yongtan, Pyeongchang, and Mungyeong groups (Choi et al., 1998). Among these, the Taebaek Group is notable for its well-preserved outcrop sections and abundant fossils, allowing the establishment of detailed lithostratigraphy and biostratigraphy (Choi et al., 2004; Choi and Chough, 2005; Kwon et al., 2006). The group composed of a wide variety of lithologic units such as coarse siliciclastics (Jangsan and Dongjeom formations), fine siliciclastics (Myobong, Sesong, and Jigunsan formations), mixed siliciclastic-carbonate rocks (Hwajeol and Dumugol formations), and carbonates (Daegi, Makgol, and Duwibong formations).

The Sesong Formation was identified as a separate siliciclastic unit between the Daegi and Hwajeol formations in the early geologic mapping era (Kobayashi, 1935; Kobayashi, 1966), but later it was degraded to a member of the Hwajeol Formation (GICTR, 1962; Cheong et al., 1969). Recent studies have confirmed the formation rank of the Sesong unit through analyses of unique lithology (Joo and Ryu, 2012), trilobite biostratigraphy (Sohn and Choi, 2005; Park et al., 2009; Park and Choi, 2011; Park et al., 2012), and carbon isotope stratigraphy (Lim et al., 2015). The Sesong Formation exhibits two lithologic divisions: a lower part composed dominantly of nodule-bearing shale and laminated very fine- to fine-grained sandstone and an upper part characterized by fine- to medium-grained sandstone (Joo and Ryu, 2012). Additionally, seven trilobite biozones have been established within the formation (Kobayashi, 1935; Park and Choi, 2011; Park et al., 2012, Choi et al., 2016). The Sesong Formation was interpreted to have been deposited in offshore, offshore transition, and lower shoreface environments and the changes in the depositional environment were controlled mainly by

relative sea-level fluctuations (Joo and Ryu, 2012). Notably, an interval representing the SPICE (Steptoean Positive Carbon Isotope Excursion) event, concurrent with a late Cambrian eustatic sea-level fall (Saltzman et al., 2004; Chen et al., 2012), was reported within the Sesong Formation (Lim et al., 2015). However, the precise origin and sedimentary processes responsible for the sandstone in the upper section of the Sesong Formation remain enigmatic. To interpret the depositional environment clearly, the study undertook sedimentary facies and ichnofacies analyses from a drill core and outcrops of the Sesong Formation.

The study also examined a newly discovered limestone conglomerate-microbialite mixed bed and dendrolite bioherms in the middle Sesong Formation to gain insights into the depositional setting. Microbialites are unique organosedimentary deposits formed through the trapping and binding of detrital sediment by benthic microbial communities and through mineral precipitation induced by microbial communities (Burne and Moore, 1987; Riding, 2000). They can be classified into four types based on their mesostructures: stromatolites with laminated structures, thrombolites with clotted fabrics, leiolites with structureless features, and dendrolites characterized by bush-like dendritic fabrics (Riding, 1991a, 2000, 2011a). Dendrolites, specifically, have a non-laminated mesostructure consisting of large clots formed by isolated clusters of calcimicrobes (Riding, 2000; Howell et al., 2011, Suosaari et al., 2018). The latter part of this thesis aims to provide detailed sedimentary and deformational structures of the limestone conglomerate on which the dendrolite bioherms inhabited. The result will give the comprehensive implication of the deformed conglomerate and dendrolite bed on a Cambrian global event and the depositional responses.

2. Geologic Setting and Previous Works

The Taebaeksan Basin occupies the central-eastern part of the Korean Peninsula. The basin has a thick succession of mixed siliciclastic-carbonate sedimentary rocks which have been subdivided into Joseon and Pyeongan supergroups (Chough et al., 2000). The Joseon Supergroup was deposited in the early Paleozoic (Cambrian-Ordovician) and is composed of a mixed sequence of sandstone, shale, and shallow marine carbonate deposited in the marginal marine environment whereas the overlying Pyeongan Supergroup consists mainly of terrestrial sandstone, shale, and minor carbonate which was formed in the marginal marine to nonmarine environment in late Paleozoic (Carboniferous-Permian) to early Mesozoic. The Joseon Supergroup rests unconformably on the Precambrian granitic gneiss and metasedimentary rocks and is unconformably overlain by sedimentary rocks of the Pyeongan Supergroup (Chough et al., 2000). The Joseon Supergroup has been divided into five lithologic units: Taebaek, Yeongwol, Yongtan, Pyeongchang, and Mungyeong groups.

The Taebaek Group is exposed in the Taebaek and Samcheok areas, the eastern part of the Taebaeksan Basin, and is well stratified following the southern limb of the Baegunsan Syncline (Fig. 1) (Chough et al., 2000). The group has been divided into the Jikdong (Cambrian) and the Sangdong subgroups (Ordovician). The Jikdong Subgroup consists of the Jangsan, Myobong, Daegi, Sesong, and Hwajeol formations, and the Sangdong Subgroup consists of the Dongjeom, Dumugol, Makgol, Jigunsan, and Duwibong formations in ascending order (Fig. 2) (Kobayashi, 1966; Choi, 1998; Lee, 2014). The Cambrian-Ordovician boundary is in the lower part of the Dongjeom Formation. The Yeongweol Group is located in the Yeongwol area and occupies the western part of the Taebaeksan Basin, bounded east by the Deokpori thrust (Choi

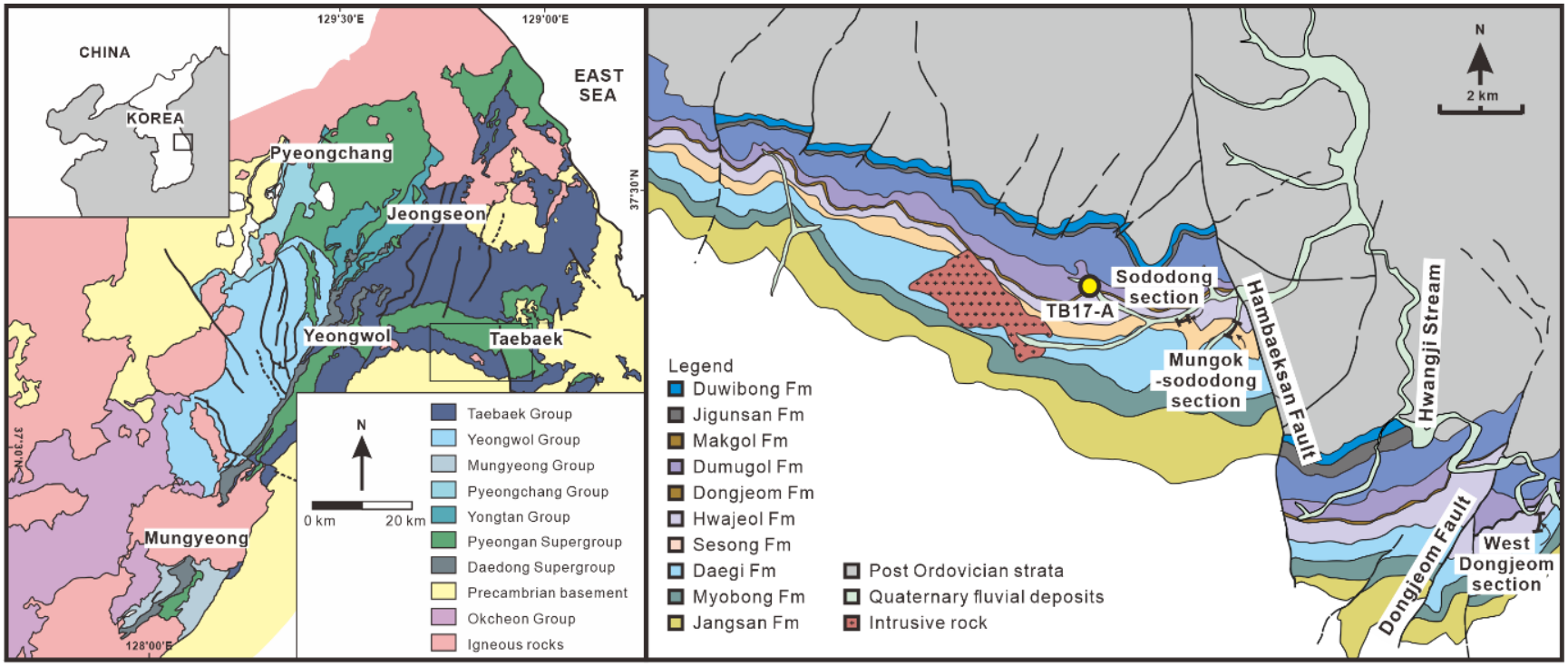

Figure 1. Geologic map of Taebaek area. Circles mark the location of the measured section (modified after KIGAM (2023)).

The Pyeongan Supergroup is grey-colored.

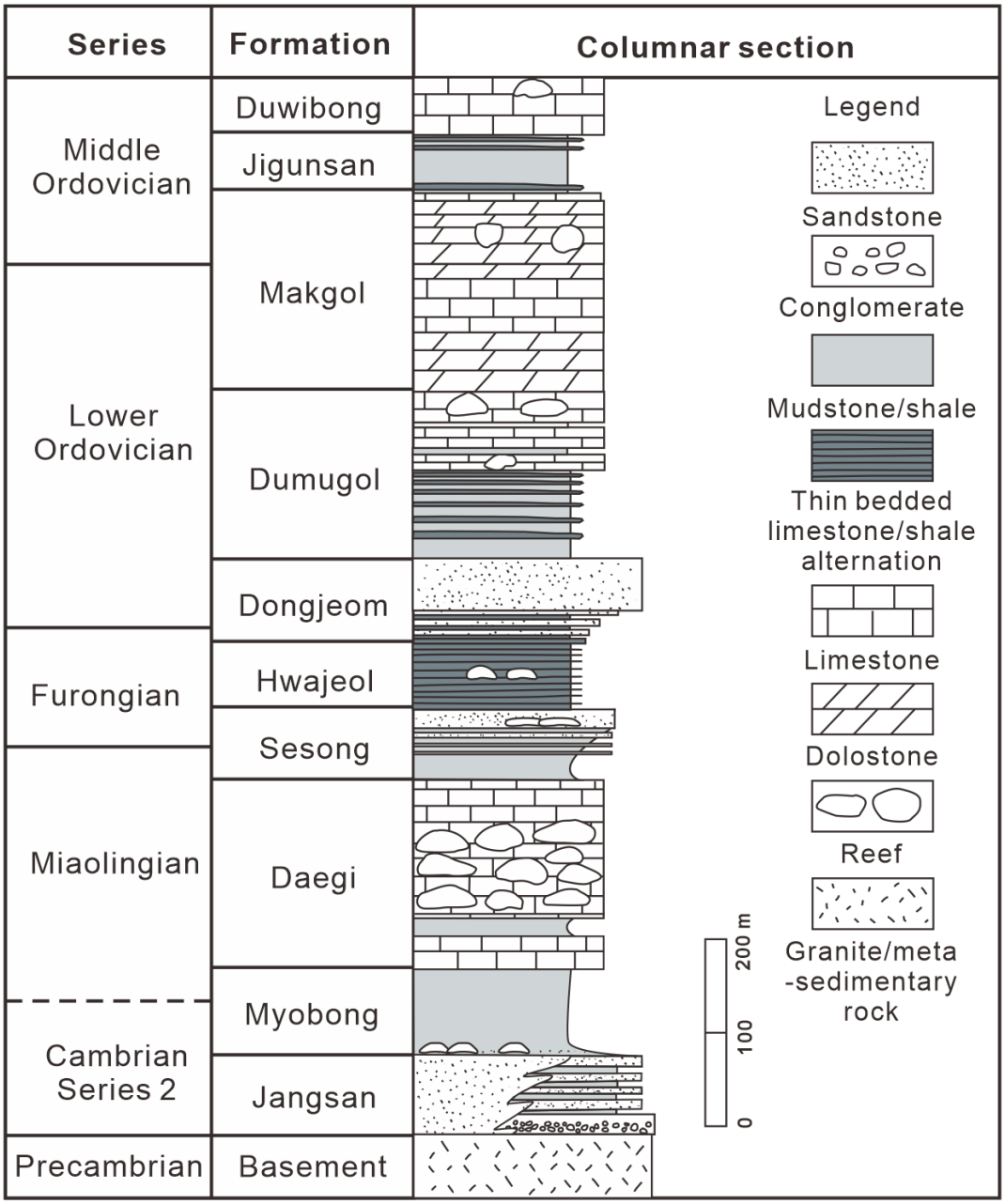

Figure 2. Stratigraphic summary of the Taebaek Group. Stratigraphic locations of microbialites are marked with arrows. The red arrow indicates stratigraphic position of the dendrolite bioherm in the Sesong Formation (modified after Lee et al., 2016).

and Chough, 2005). It is subdivided into the Sambangsan, Machari, Wagok, Mungok, and Yeongheung formations, and the geologic age of the group ranges from the middle Cambrian to late Ordovician (Kobayashi, 1966; Choi, 1998). The Mungyeong Group is the southernmost part of the basin exposed in the Mungyeong area. It was bounded east by the Seokhyeon thrust and west by the Sangnaeri thrust (Kobayashi et al., 1942). This group has been divided into the Gurangni, Maseong, Hanaeri, Seokgyori, Jeongni, and Dotanni formations in ascending order (Aoti, 1942; Kobayashi, 1966), but later workers failed to identify this lithostratigraphy (Um et al., 1977; Lee, 1987; Lee et al., 1993; Choi, 1998; Lee, 2006). The Yongtan and the Pyeongchang groups are exposed respectively in the Jeongseon and Pyeongchang areas, the northern part of the Taebaeksan Basin. The stratigraphy and relationship of these groups to the others are still debatable.

Kobayashi (1935) originally designated the stratigraphic names of the Lower Paleozoic strata in the Taebaek and Samcheok areas based on their lithostratigraphy and biostratigraphy. But the Geological Investigation Corp of Taebaegsan Region (GICTR) (1962) and Cheong (1969) lowered the rank of the Hwajeol unit from group to formation and considered the Sesong Formation as the lowermost member of the Hwajeol Formation, which was named Sesong Marl. Meanwhile, Choi et a1. (2004), and Choi and Chough (2005) regarded the Sesong Marl as a lithologically distinctive formation. The Sesong Marl (lower Hwajeol member) and Hwajeol Quartzite are considered the Sesong Formation. The formation is thought of as a result of a single transgressive sequence whose depositional environment is interpreted as a gently inclined inner or outer shelf (Kwon et al., 2006). The frequency and proportion of the intercalated sandstone layers are higher in the Sangdong area than in the Dongjeom and Seokgaejae areas (Kwon et al., 2006). More recently, detailed sedimentary facies analysis in the Dongjeom area found that the depositional environment changed from the outer shelf to the inner shelf as the relative sea-level varies (Joo and Ryu, 2012). The maximum value of stable carbon isotope in the Sesong Formation coincides with the correlative conformity caused by relative sea-level fall (Lim et al., 2015).

The Sesong Formation is composed mainly of nodule-bearing shale with intercalation of limestone conglomerate in the lower part; fine- to medium-grained sandstone with occasional intercalation of limestone conglomerate in the middle part and; silt to fine-grained sandstone with limestone conglomerate in the upper part (Park et al., 2012). The lower boundary of the Sesong Formation is characterized by an abrupt and sharp facies change from limestone of the Daegi Formation to nodular shale. The upper boundary of the formation is located in a transitional zone with a facies change from fine-grained sandstone to limestone-shale couplets of the Hwajeol Formation (Park et al., 2012).

3. Methods and Materials

Detailed facies analysis of drill core (TA-17A)

Sedimentary structures, bedding surfaces, and bioturbation fabrics of the Sesong Formation are well preserved in the drill core from Hyeoldong, Taebaek-si. The total length of the drill core is about 120 m. Facies analysis of the drill core is carried out on a millimeter scale. Thin sections are made from samples that have specific sedimentary or biogenic features. Based on the facies variation of the core, columnar drawing work has been done on a scale of 1: 10, 1:20, and 1:100. The standard legend was originally set in the core and applied to the outcrop observations. One hundred thirty-six thin sections were made to closely observe and compare the composition and structures of the sedimentary rock. Additionally, the thin sections were used to verify the boundary characteristics between the facies.

Outcrop observation

Three outcrop sections in the Taebaek area are mainly observed: 1) the West-Dongjeom section, 2) the Mungok-Sododong section, and 3) the Sododong section. Overall sedimentary facies and architecture of the beds were observed on weathered surfaces. Columnar drawing work and field sketch has been done on a scale of 1:20. Hand grinders were used to eliminate lichens covering the surfaces of the outcrop and see the fresh surfaces. Every section commonly has thick sandstone units that are bioturbated or parallelly laminated and are intercalated with a bioclastic pack to grainstone or limestone pebble conglomerate. However, each section is correlated to different parts of the core. Detailed information on each section is stated below.

Bioturbation Index and Ichnofacies

If sedimentary rocks display disruptions, these may arise from various factors, including soft sediment deformation, tectonic activity, and biogenic disturbances. The measured cores and outcrop sections have many intermingled sandstone intervals, which are assumed to be reworked

by organisms after sedimentation. The bioturbation intensity (Bioturbation Index) and tendency were identified by observing the bioturbated sandstone samples from the outcrops and drill core. Integrating this data with the lithostratigraphic information can lead to a more precise and systematic interpretation of paleogeography and paleoenvironmental conditions.

4. Description and Interpretation of Sedimentary Facies

4.1. Homogeneous mudstone (Facies Mh)

4.1.1. Description

This facies is represented by dark gray-colored homogeneous mudstones (Fig. 3). Grain size ranges from coarse- to fine-grained siltstone (0.0078 mm-0.0625 mm). Internal structures and fossil fragments are not found. The thickness of the bedding varies from a few millimeters to decimeters. The facies occasionally has a sharp and irregular lower boundary. The upper boundary is either sharp or graded sparsely.

4.1.2. Interpretation

Homogeneous mudstone facies can occur in regions far from the sediment source. The predominance of fine-grained silt-rich mudstones and the absence of traction-generated structures suggest that the facies was deposited by suspension settling in low-energy conditions (Van Houten and Bhattacharyya, 1982; Macquaker and Gawthorpe, 1993; Choi et al., 2004).

4.2. Bioturbated mudstone (Facies Mb)

4.2.1. Description

This facies is characterized by a frequent alternation of very thin, dark gray mud to minor siltstone and thin sandstone, with modifications by burrows (Fig. 4). The intensity and type of the bioturbation vary; sparsely bioturbated mud to siltstones contain well-preserved horizontal to sub-horizontal burrows on the surface of laminae, and as bioturbation intensity increases individual burrows of strongly bioturbated mud to siltstones are hardly recognized.

4.2.2. Interpretation

Mudstones of this facies were deposited originally with planar laminas and were modified by bioturbation. Deposition of mudstone occurs in a quiet depositional environment and the predominance of horizontal burrows indicates an environment that has a relatively low rate of sedimentation. Seasonal change of wave energy results in the alternation of sandstone and

mudstone.

4.3. Laminated sandstone (Facies Sl)

4.3.1. Description

This facies is represented by gray or brown colored, parallelly laminated sandstone (Fig. 5). The grain size usually ranges from very fine-grained sandstone (0.0625-0.125mm) to medium-grained sandstone (0.25-0.5mm). The laminations are evident in the heterolithic intervals but are crudely stratified in the sandy intervals. The sorting following the lamination is good and the lamination interbedded with some normally graded beddings occasionally contains some calcareous grains in the lower part. The coarser part of the facies includes calcareous grains and shelly fragments that are aligned with lamination. This calcareous layer has undulatory upper surfaces. Small-scale wave ripples and cm-scale normal gradings occasionally occupy above the coarser part and below the typical parallelly laminated sandstone. Very fine- to fine-grained sandstone of this facies contains elliptical or ovoid carbonate concretion without bioclast.

4.3.2. Interpretation

The planar lamination of sandstones with distinct heterolithic composition is considered to be deposited by storm current below the storm wave base (Choi et al., 2004; Kwon et al., 2006; Joo and Ryu, 2012). Coarse, bioclastic sandstone layers and overlying sandstone beds displaying ripple laminations are considered high-energy event beds induced by storm density currents. The storm current that has a high- mean flow velocity forms the upper flow regime. The frequent intercalation of siltstone within the sandstone indicates fluctuation in flow velocity.

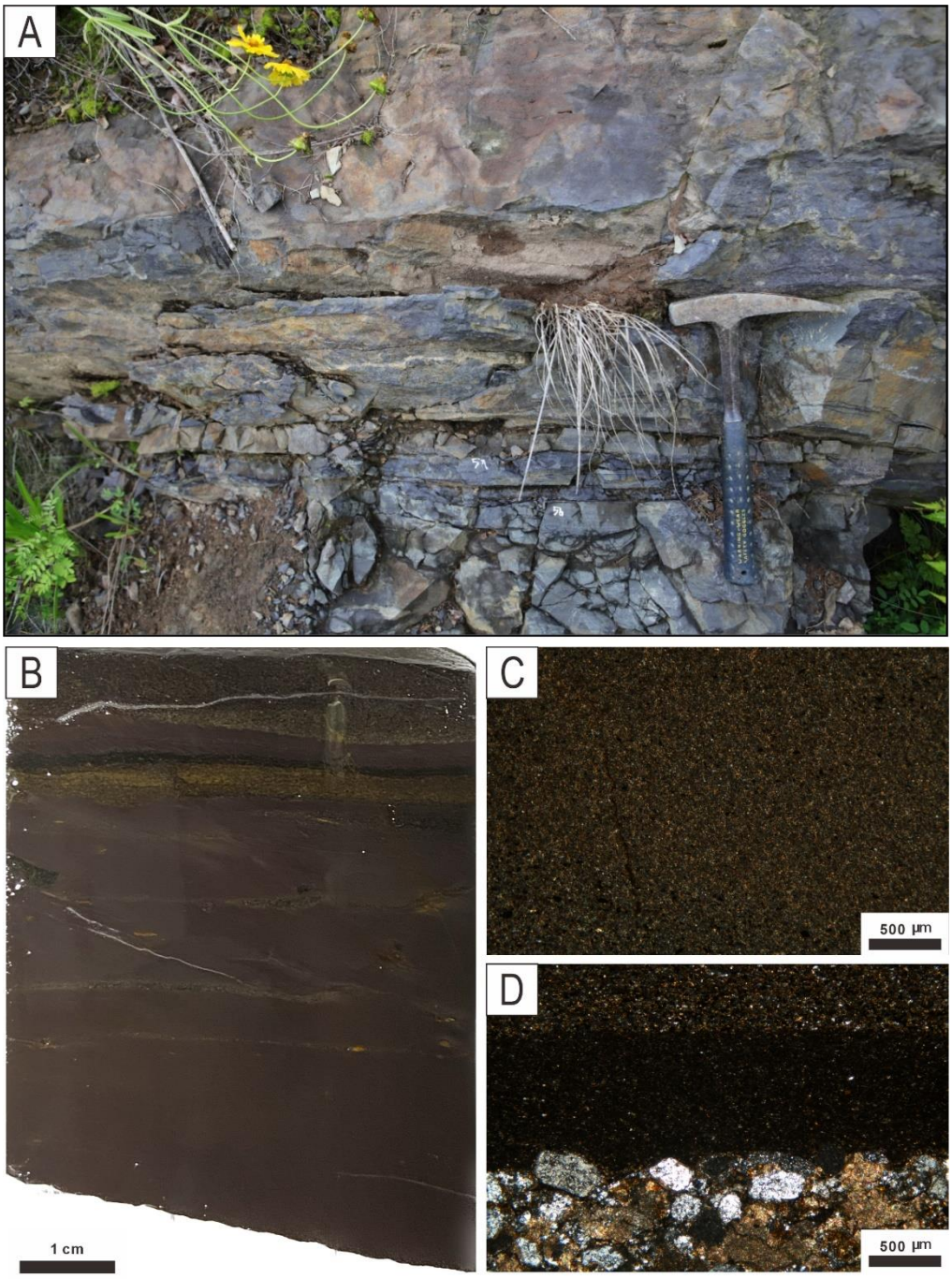

Figure 3. Photographs of homogeneous mudstone (Facies Mh). (A) Homogeneous mudstone is thinly interbedded within laminated sandstone (Sl) and bioturbated sandstone (Sb). West-dongjeom section. Hammer for scale is 27 cm long. (B) Homogeneous mudstone in the TB17-A core. (C) Photomicrograph of homogeneous mudstone. (D) Photomicrograph showing vertical succession of medium-grained sandstone, homogeneous mudstone, and siltstone.

4.4. Bioturbated sandstone (Facies Sb)

4.4.1. Description

This facies consists of sparsely to strongly bioturbated very fine-grained to medium-grained sandstone with alternating thin mudstone layers (Fig. 6). Primary sedimentary structures had been deformed and displaced by bioturbation structures. Horizontal/sub-horizontal burrows and vertical/sub-vertical burrows coexist. Thin bioturbated mudstone (Facies Mb) layers comparting bioturbated sandstone beds show variable bioturbation intensity from 0 to 4. The burrows observed in the mudstone layers were not destroyed and were maintained as open burrows. The diversity of trace fossils is enhanced with an increased bioturbation index. Detailed classification following the bioturbation intensity (Bioturbation Index), ichnofabric types, and their assemblages will be explained in a separate section.

4.4.2. Interpretation

Various trace fossils made most likely by benthic invertebrates indicate a subtidal environment. Preservation of the original burrowing in the mudstone layer means that the substrate solidity was firm enough to resist deformation. Maintenance of the original burrowing form means that the substrate solidity was firm enough to resist deformation. Different degree of bioturbation implies that there was certain grading in physicochemical conditions within the depositional environment, which include sedimentation rate, agitation of surface sediment, and so on. Bioturbated sandstones with gradational increases of BI without a notable variation in grain size can be interpreted as a result of deposition under the lowered sedimentation rate.

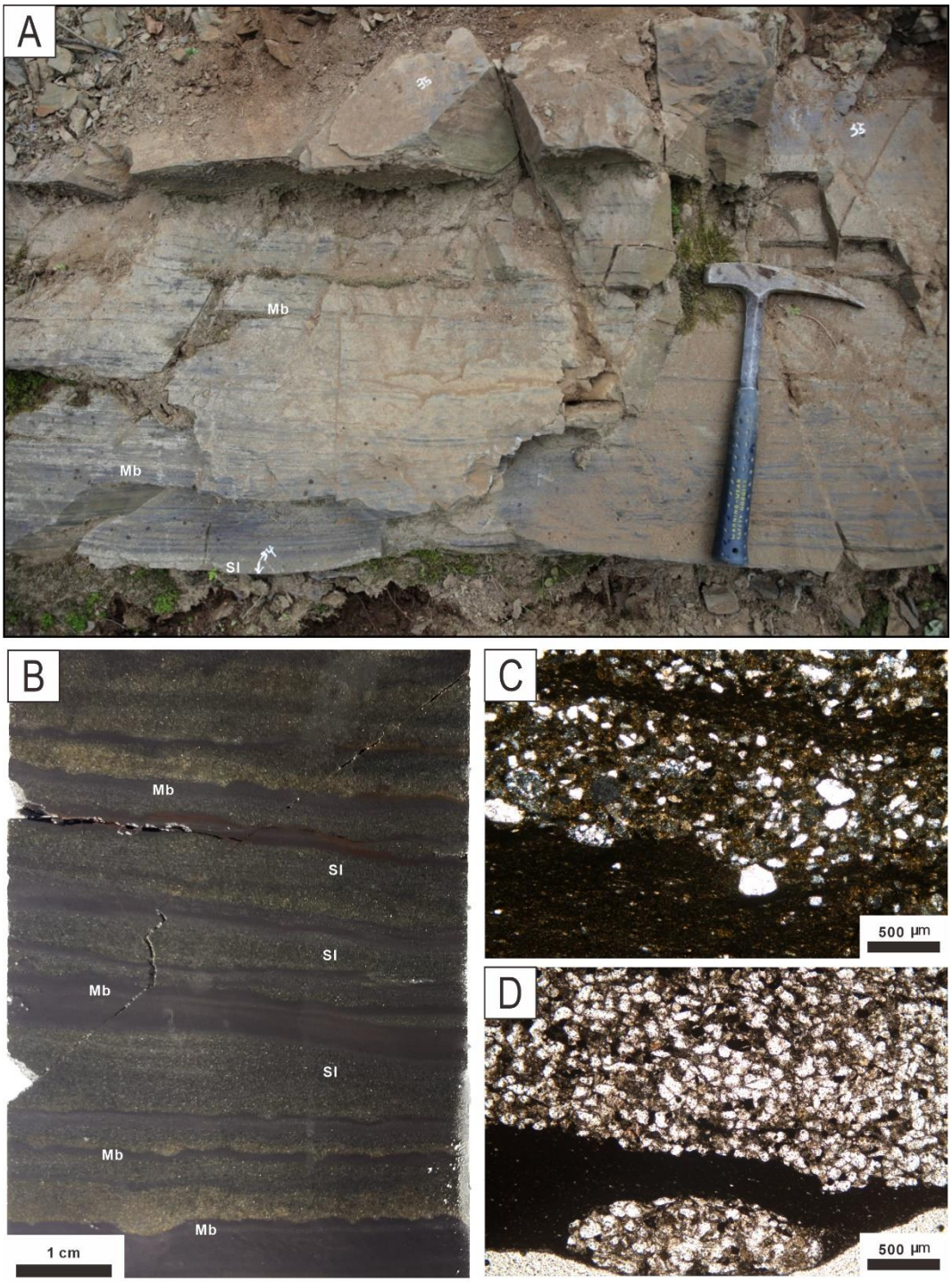

Figure 4. Photographs of bioturbated mudstone (Facies Mb). (A) Intercalation of bioturbated mudstone and bioturbated sandstone in the TB17-A core. (B) Photomicrograph of bioturbated mudstone and sandstone of West-dongjeom section. (C) Photomicrograph of an isolated burrow and sand infill of bioturbated mudstone.

4.5. Massive sandstone (Facies Sm)

4.5.1. Description

This facies mainly consists of moderately to well-sorted and subrounded to well-rounded fine- to medium-grained quartzose sandstone with rare internal structures (Fig. 7). The thickness of the facies is less than a few centimeters. Rare faint parallel lamination formed by subtle changes in grainsize (Fig. 7B). Coarse fragmented bioclasts are randomly dispersed in this facies or sometimes aligned along certain horizons resulting in formation of relatively coarser lamina. Muddy or silty laminae commonly overlies the facies with a sharp or gradual boundary. Fossiliferous calcareous concretions occur in some parts of the facies and result in undulatory geometry of the facies units.

4.5.2. Interpretation

The massive sandstones are generally formed by the rapid deposition of suspended sands or the destruction of primary sedimentary structures resulting from the maximum bioturbation intensity (Collinson et al., 2006). The faint lamination without remnant burrow structures in this facies supports the rapid deposition. Thin facies units and frequent alternation with mudstone facies indicate that the deposition took place in a low-energy setting such as a distal part of the system.

4.6. Calcareous sandstone (Facies Sc)

4.6.1. Description

The facies is composed of very fine- to fine-grained quartzose sand and minor coarse- to very coarse-grained, white-colored calcareous skeletal grain with some micritic matrices (Fig.

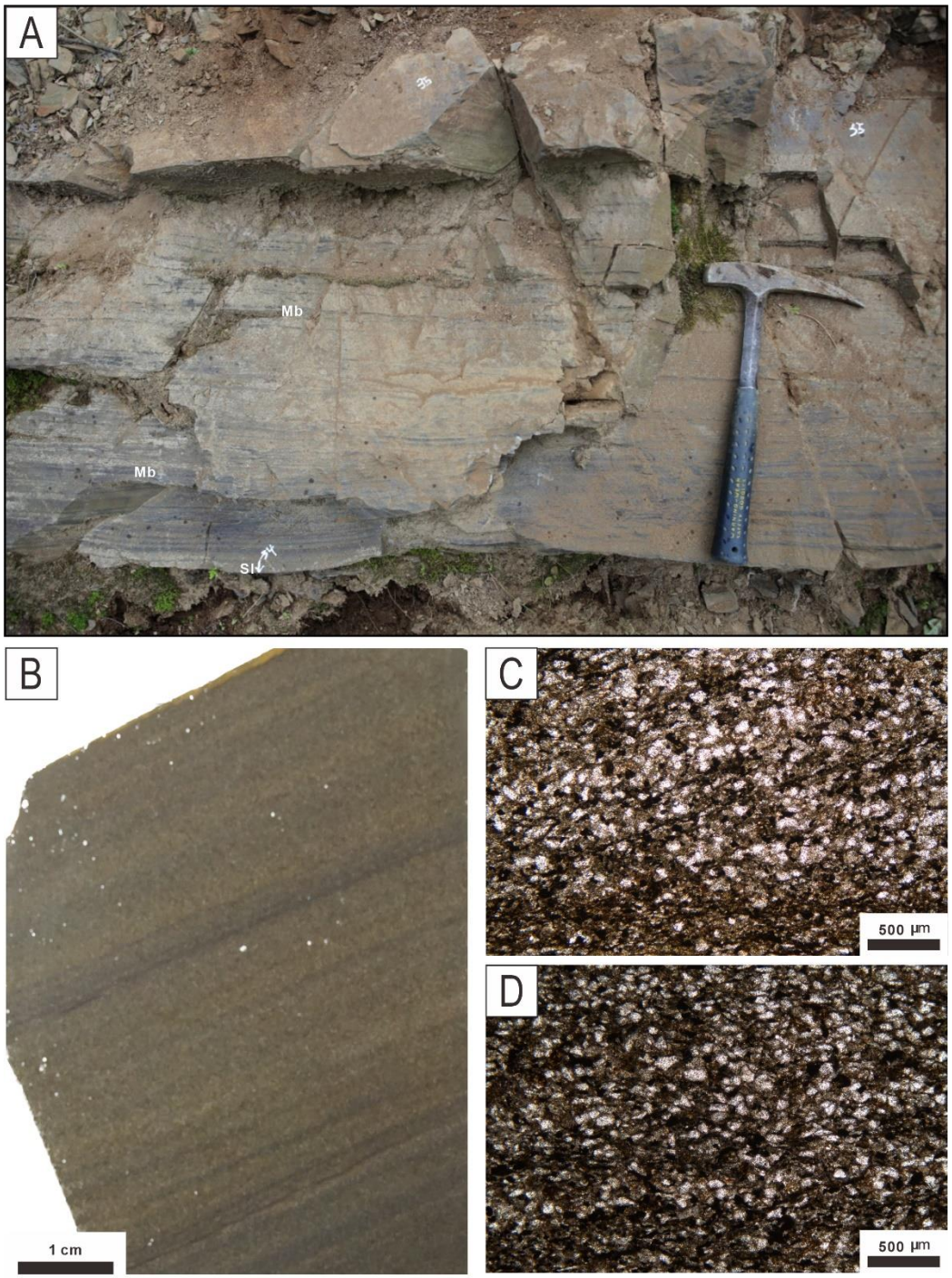

Figure 5. Photographs of laminated sandstone (Facies Sl). (A) Intercalation of laminated sandstone and siltstone. West-dongjeom section. Hammer for scale is 27 cm long. (B) Laminated sandstone in the TB17-A core. (C), (D) Photomicrographs of laminated sandstone.

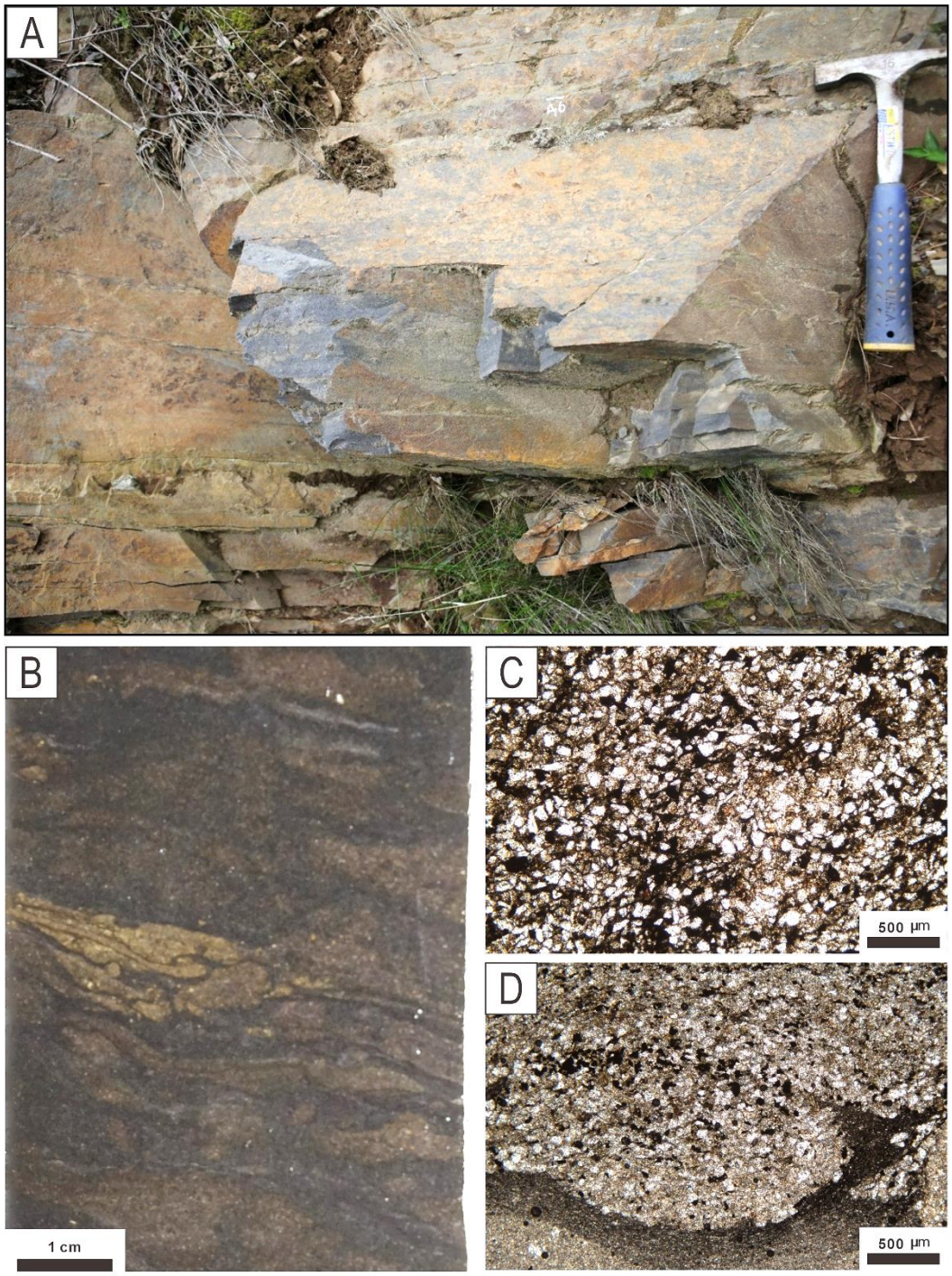

Figure 6. Photographs of bioturbated sandstone (Facies Sb). (A) Bioturbated fine-grained sandstone exposed West-dongjeom section. Hammer for scale is 27 cm long. (B) Bioturbated sandstone in the TB17-A core. (C) Photomicrograph of strongly bioturbated sandstone and destroyed primary lamination. (D) Photomicrograph of moderately bioturbated sandstone horizontal burrow.

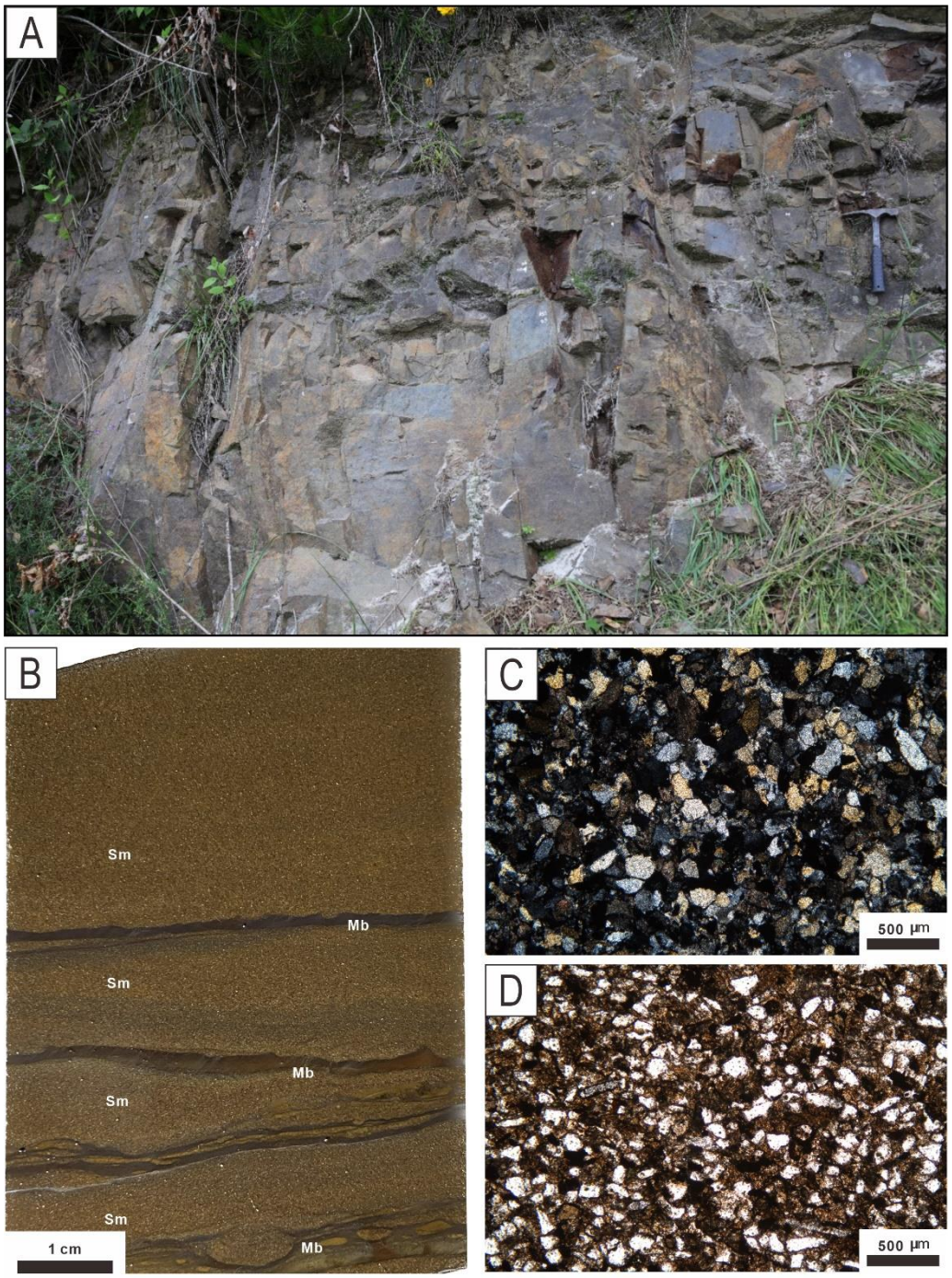

Figure 7. Photographs of massive sandstone (Facies Sb). (A) Bioturbated sandstone and thinly intercalated bioturbated mudstone. West-dongjeom section. Hammer for scale is 27 cm long. (B) Massive sandstone and thinly intercalated bioturbated mudstone in the TB17-A core. (C) Photomicrograph of fine-grained massive sandstone (cross-polarized light, XPL). (D) Photomicrograph of fine-grained sandstone and micritic matrix.

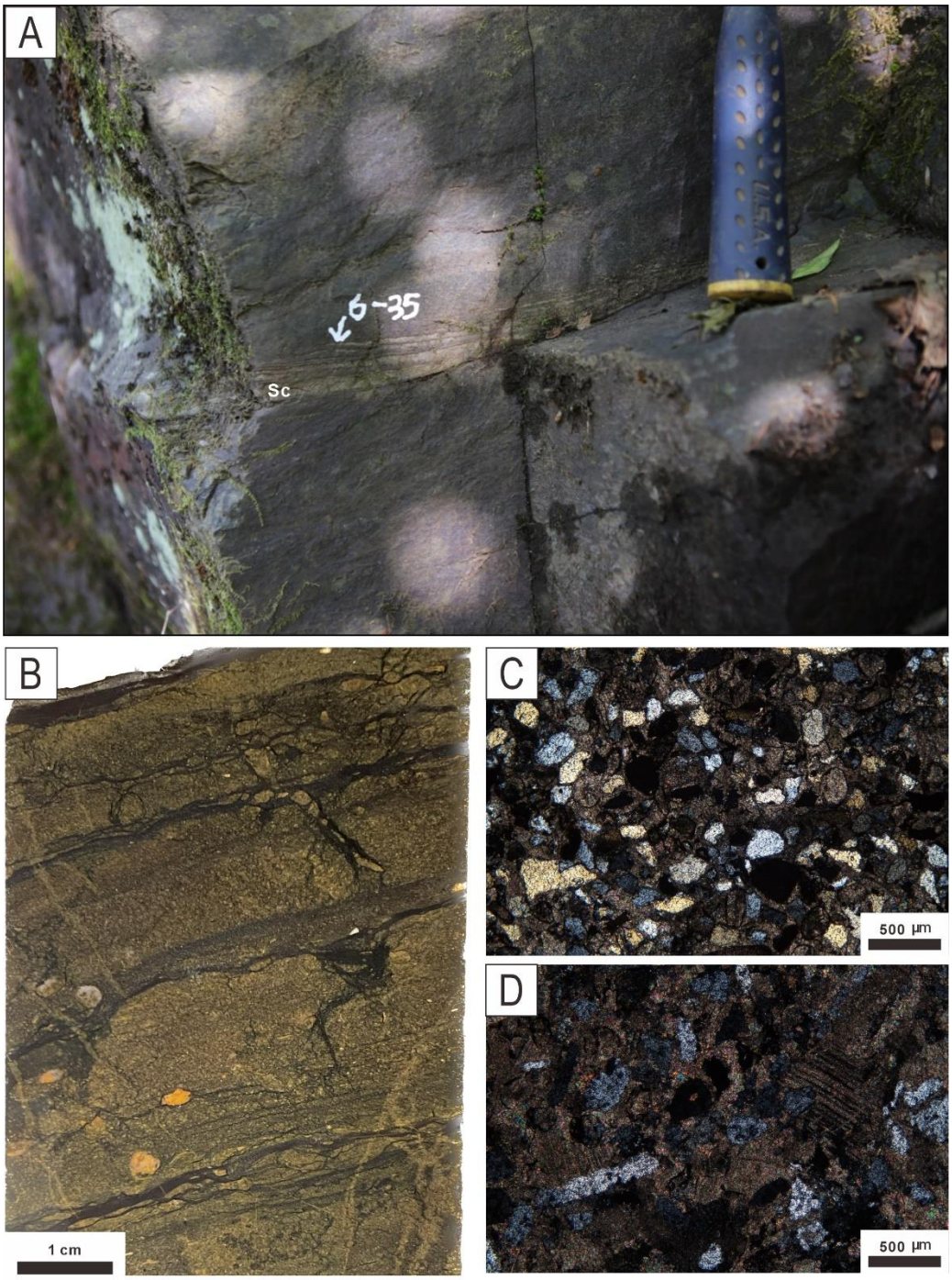

Figure 8. Photographs of calcareous sandstone (Facies Sc). (A) Calcareous sandstone layer in the Mungok-sododong section. Thickness of the marked calcareous sandstone layer is about 2 cm. (B) Calcareous sandstone in the TB17-A core. (C) Photomicrograph of calcareous sandstone consists of medium to fine-grained quartz sand and micrite matrix (XPL). (D) Photomicrograph of calcite cemented massive sandstone (XPL).

8). Calcite cementation of the pore spaces and/or micritic matrices makes sandstone calcareous. Therefore, this facies may be subdivided into calcite cemented sandstone (Scc) and micritic sandstone (Scm). Calcite-cemented sandstone occurs as a thin sheet (1-1.5 cm), lenticular, or nodular form in massive and laminated sandstone dominant intervals. The thickness of micritic sandstone is 4-8 cm on average.

4.6.2. Interpretation

Highly abraded carbonate bioclasts indicate prolonged agitation before deposition with siliclastic grains. This further suggests that the quartz grains and bioclasts were influenced by waves and currents and transported into the current position. Micrite in the pore space of sandstone either represents deposition in a quiet environment or micritic cement formed during diagenesis.

4.7. Massive pack to grainstone (Facies P-G)

4.7.1. Description

This facies is characterized by the reddish grey colored sandy and bioclastic pack to grainstone (Fig. 9). The arrangement of bioclasts such as crinoids, brachiopods, trilobites, and echinoids is somewhat chaotic, and thin shale laminae are frequently intercalated with this facies. Peloidal components of diverse sizes such as intraclast are common constituents of the facies.

4.7.2. Interpretation

This facies is deposited by sediment eroded and reworked by wave and storm currents (Kreisa, 1981). The original bioclastic pack to grainstone beds deposited in a shallow subtidal platform were eroded by high energy currents. The storm currents induced the reworked calcareous skeletal grains to more distal area.

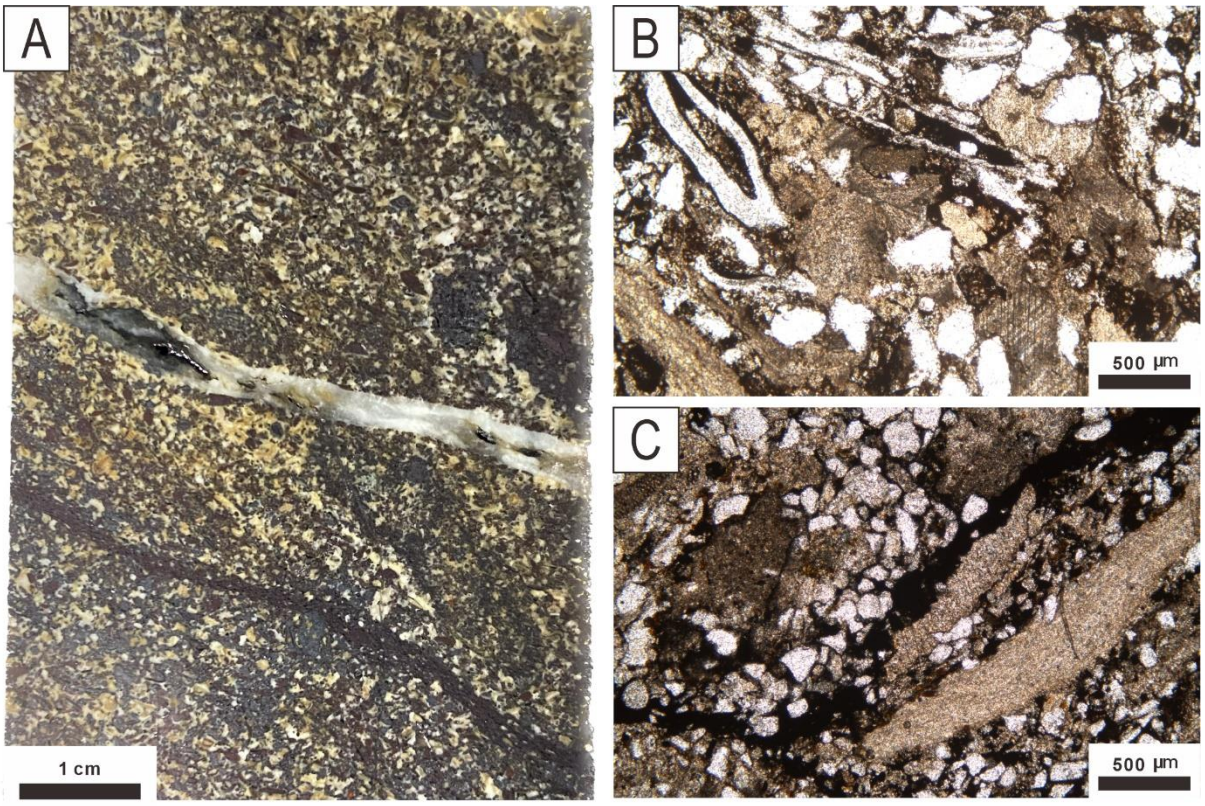

Figure 9. Photographs of massive pack to grainstone (Facies P-G). (A) Massive pack to grainstone in the TB17-A core. (B) Photomicrograph of bioclasts and quartz sand grains. Interspace between grains is cemented with calcite. (C) Photomicrograph of brachiopods shell and fine-grained quartz sand grains in the sandy part of pack to grainstone.

4.8. Limestone pebble conglomerate (Facies Clp)

4.8.1. Description

This facies is represented by various shapes, packing, and textures of lime pebble clasts (Fig. 10). The matrices usually comprise bioclastic pack-to-grainstone containing abundant fine to medium-grained quartz sand grains and occasionally contain fragments of microbial buildups, calcareous shale, and stylolites. The shape of limestone pebble clasts is spherical to elliptical and even irregular due to bioerosion. Most of the clasts are well-rounded and well-sorted. The limestone pebble clasts show a subtle pinkish or purplish color.

4.8.2. Interpretation

Limestone clasts composing this facies originated from semi-consolidated sediments eroded, winnowed, and transported by wave and storm currents (Kwon et al., 2002; Myrow et al., 2004). The clasts are resedimented on the lower part of the shelf by storm events. Well-rounded clasts are indicative of reworking and winnowing.

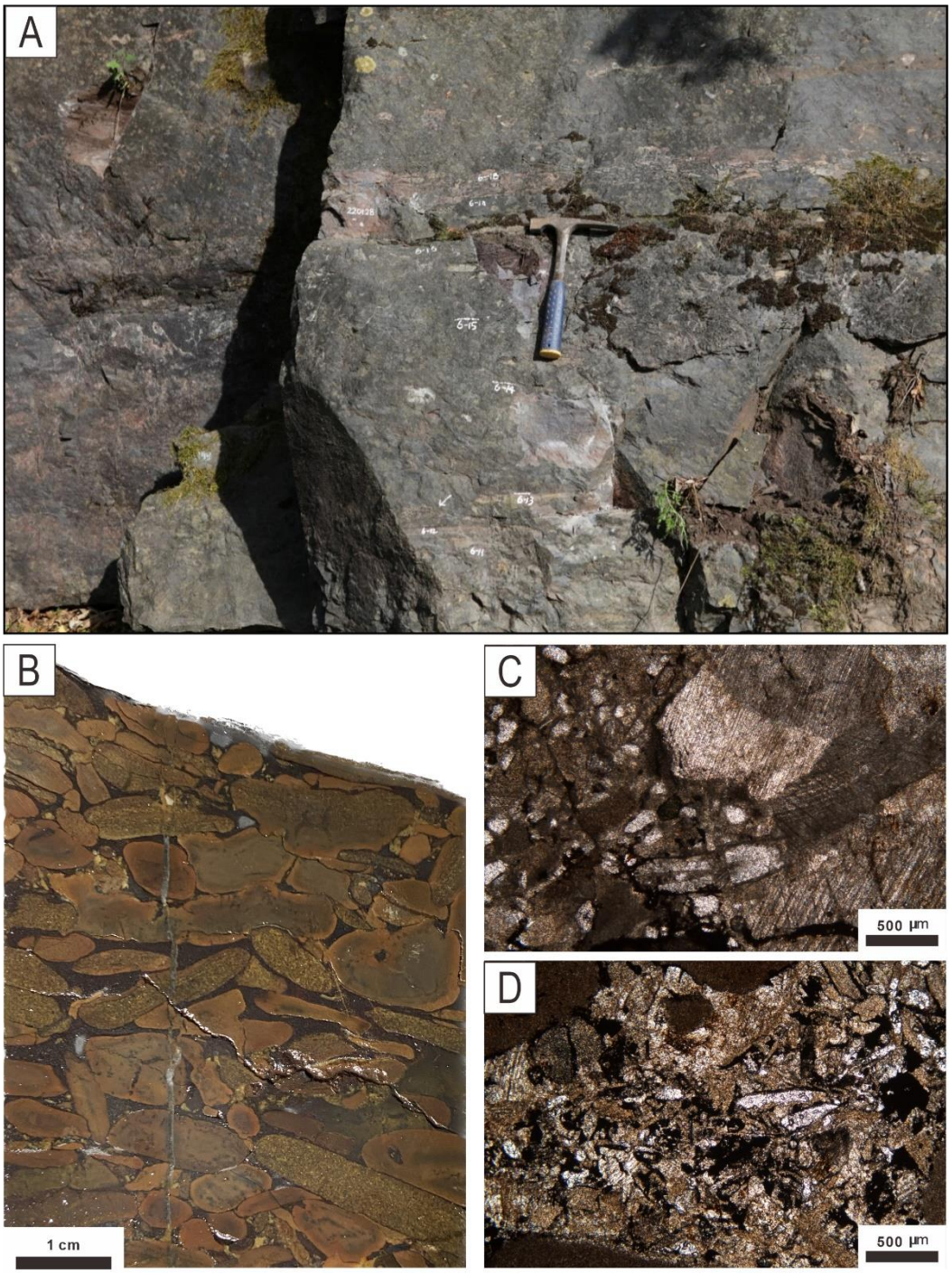

Figure 10. Photographs of limestone pebble conglomerate (Facies Clp). (A) Limestone pebble conglomerate bed marked with white arrow. Sododong section. Hammer for scale is 27 cm long. (B) Limestone pebble conglomerate in the TB17-A core. (C) Photomicrograph of sparry calcite, fine-grained quartz and bioclasts of limestone pebble conglomerate. (D) Photomicrograph of lime mud clasts marked with white arrows and interspace filled with pack to grainstone matrix.

5. Facies Associations

Based on the detailed measurement of TB17-A drill core and outcrop sections of the upper part of the Sesong Formation, three facies associations are recognized: (1) Facies Association 1 (upper offshore transition), (2) Facies Association 2 (middle offshore transition), and (3) Facies Association 3 (lower offshore transition) (Table 2).

5.1. Facies Association 1

Facies Association 1 is characterized by the interbedding of non-amalgamated bioturbated sandstone (Facies Sb), bioturbated mudstone (Facies Mb), massive pack to grainstone (Facies P-G), and limestone conglomerate (Facies Cl) layers (Fig. 11). Fine-grained bioturbated sandstone and bioturbated mudstone facies of this association show

a relatively high degree of Bioturbation Index (BI 3-5) on average. Bioturbation Index tends to decrease toward the top of the association. Various types of bioturbation occur in this association, and the assemblage exhibits a range of ichnofossils, including *Planolites, Palaeophycus, Arenicolites,* and *Teichichnus*. Calcareous sandstone (Facies Sc), laminated sandstone (Facies Sl), and massive sandstone (Facies Sm) are occasionally interbedded as minor components.

The predominance of sandstone facies suggests proximity to the shallow coastal environments. Lack of cross-laminations indicating active wave agitation or wave-generated currents is suggestive of deposition below the fairweather wave base. The high degree of bioturbation interpreted as an optimal condition of animal activities also supports deposition out of shoreface environments where restless reworking hampers the formation of dense bioturbation.

Facies Association	Constituent Facies	BI	Average sandstone grain size	Interpretation
FA 1	Bioturbated sandstone (Sb), Bioturbated mudstone (Mb), Massive pack to grainestone (P-G), Limestone conglomerate (Clp)	Intense (3-5)	Medium to fine	Upper offshore transition
FA 2	Bioturbated sandstone (Sb), Massive sandstone (Sm), Bioturbated mudstone (Mb), Limestone conglomerate (Clp)	Moderate (2-4)	Fine	Middle offshore transition
FA 3	Laminated sandstone (Sl), Calcareous sandstone (Sc), Massive sandstone (Sm), Homogeneous mudstone (Mh)	Moderate to Sparse (1-3)	Fine to very fine	Lower offshore transition

Table 2. Facies associations of the upper Sesong Formation.

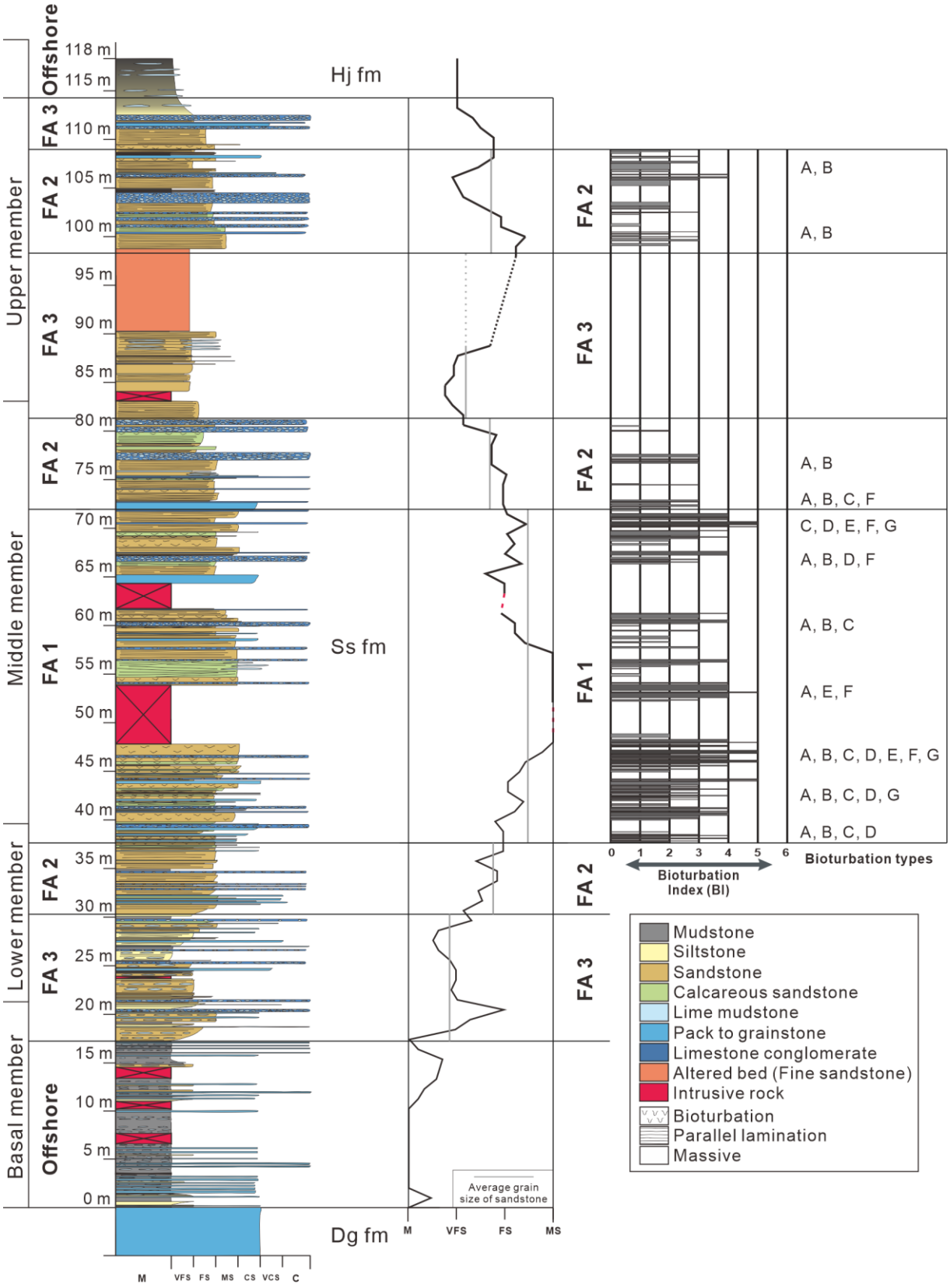

Figure 11. Vertical facies, grain size, and bioturbation index change within the Sesong Formation.

Frequent intercalation of mud to siltstone and moderate to intense degree of bioturbation indicate a relatively low sedimentation rate. Together with the characteristics that lack coarse-grained sandstone, this facies association is interpreted as a proximal offshore transition where waves and currents are less effective.

5.2. Facies Association 2

Facies Association 2 is mainly composed of bioturbated sandstone (Facies Sb), massive sandstone (Facies Sm), bioturbated mudstone (Facies Mb), and limestone pebble conglomerate (Facies Clp). Minor laminated sandstone (Facies Sl) is intercalated within the bioturbated sandstone (Fig. 11). Sandstones of FA 2 are fine-grained sandstone which is intermediate between FA 1 and FA 3. Bioturbated sandstone and mudstone show moderate bioturbation intensity (BI 2-4). The diversity of burrows is smaller compared to that of FA 1. The clast of limestone conglomerate on the uppermost part of the TB17-A core consists of white to grey colored marlstone, while the general component of the clast of the underlying conglomerate is pinkish or purplish colored lime mudstone. This facies association displays an assemblage of ichnofossils such as *Planolites*, *Palaeophycus*, and *Teichichnus*.

The finer-grained sandstone (Sb, Sm) and frequent intercalation of the thin bioturbated mudstone (Mb) facies represent the middle offshore transition zone, deeper than FA1. The absence of pack-to-grainstone, which originates from shallower environments, supports that FA2 was deposited in greater water depth than FA1. Intercalated limestone conglomerates are attributed to the severe storm activities and induced off-shoreward flows, which were able to rip- up and transport coarse grains into the transition zone (Myrow et al., 2004). The smaller degree of bioturbation and decreased diversity of burrows are interpreted as reduced organism activities in the deeper part of the platform (Pemberton et al., 1992).

5.3. Facies Association 3

Facies Association 3 consists of laminated sandstone (Facies Sl), calcareous sandstone

(Facies Sc), massive sandstone (Facies Sm), and homogeneous mudstone (Facies Mh) (Fig. 11). FA 3 is well exposed in the Mungok-Sododong section. Most sandstones composing this association are very fine- to fine-grained laminated sandstones. Calcareous nodules in calcareous sandstone appear in nodular or lenticular shape and have a sharp boundary. Bioturbation is rarely observed (BI 0-1), but the upper surface of mudstone is slightly bioturbated, resulting in a gently undulating form.

The finer grain size of this association suggests a tranquil environment with little current activity. It suggests that the relative sea level rise resulted in increased water depth. It is estimated that there was an environment with high physicochemical stress as trace fossils disappeared. Considering this evidence comprehensively, the depositional environment of FA 2 is presumed to have been a lower offshore transition environment.

6. Description of Measured Sections

6.1. TB-17A drill core (ca. 70 m)

Facies analysis is mainly conducted within the TB-17A core. Facies association 1 is characterized by the high intensity of bioturbation in the sandstone beds (Fig. 11). Thin, slightly bioturbated calcareous sandstone facies are intercalated with the bioturbated sandstone facies. Carbonate facies of this division are mostly composed of massive packstone to grainstone facies and limestone pebble conglomerate facies. Facies association 2 is composed of moderately bioturbated sandstone (BI 3) and calcareous sandstone facies. The intensity of bioturbation in the sandstone beds decreases compared to FA 1, and thick limestone pebble conglomerate facies occupies instead of packstone to grainstone facies. Facies association 3 is characterized by laminated or slightly bioturbated calcareous sandstone facies. Homogeneous mudstone facies and bioturbated mud-to-siltstone facies are thinly intercalated within the sandstone facies. The intercalation of limestone pebble conglomerate facies exhibits good roundness of the clasts, while sporadic occurrences of calcareous concretions are observed within the laminated sandstone beds.

6.2. West Dongjeom Section (ca. 25 m)

The West Dongjeom section is located southeastern part of the Taebaeksan Basin, ca. 550 m west of the Dongjeom station. The section covers the middle and upper sandier part of the Sesong Formation (Fig. 12). The lower boundary of the formation, the boundary between the Daegi and Sesong formations, and the lower shaly part of the formation are not exposed or preserved in this section. The upper boundary and the uppermost transitional part between the Sesong and Hwajeol formations are absent because of the severe weathering. The West Dongjeom section mostly consists of bioturbated fine- to medium-grained sandstone facies and laminated sandstone facies. Cross-stratified calcareous sandstone facies can be found in this section. Limestone pebble conglomerate facies of 10-20 cm thickness are intercalated within the

sandstone facies. Calcareous sandstone and limestone pebble conglomerate of the lower half of the section are severely weathered compared to those of the upper half of the section.

6.3. Mungok-Sododong Section (ca. 44 m)

The Mungok-Sododong section occurs along the road from the Mungok-Sododong community service center to the Taebaek coal museum. This section covers the Sesong Formation relatively successively from the lower shaly part (20 m) to the upper sandy part (24 m) (Fig. 12). However, the uppermost part and the upper boundary of the formation were difficult to recognize either in this section. The lower nodule-bearing shale facies transitionally changes to the sandy facies with siltstone and very fine-grained sandstone. The upper sandy part comprises bioturbated sandstone (facies Sb), bioturbated mudstone (facies Mb), laminated sandstone (facies Sl), and limestone pebble conglomerate (facies Clp) (Fig. 12). The bioturbation index of the section is similar to the first division of the TB-17A drill core.

6.4. Sododong Section (ca. 10 m)

The Sododong section is the nearest section from the drill core Tb-17A, located ca. 2.8 km southeast from there. The section covers only the upper half of the formation, and the occurred thickness is about 20 m. One interesting discovery in this section is the existence of dendrolite bioherm structures in a sandstone-dominated setting (Fig. 12). The dendrolite bioherm is placed 4 m high from the bottom of the measured section. This section is composed of bioturbated sandstone (facies Sb), laminated sandstone (facies Sl), massive pack to grainstone (P-G), and limestone pebble conglomerate (facies Clp) (Fig. 12, 13).

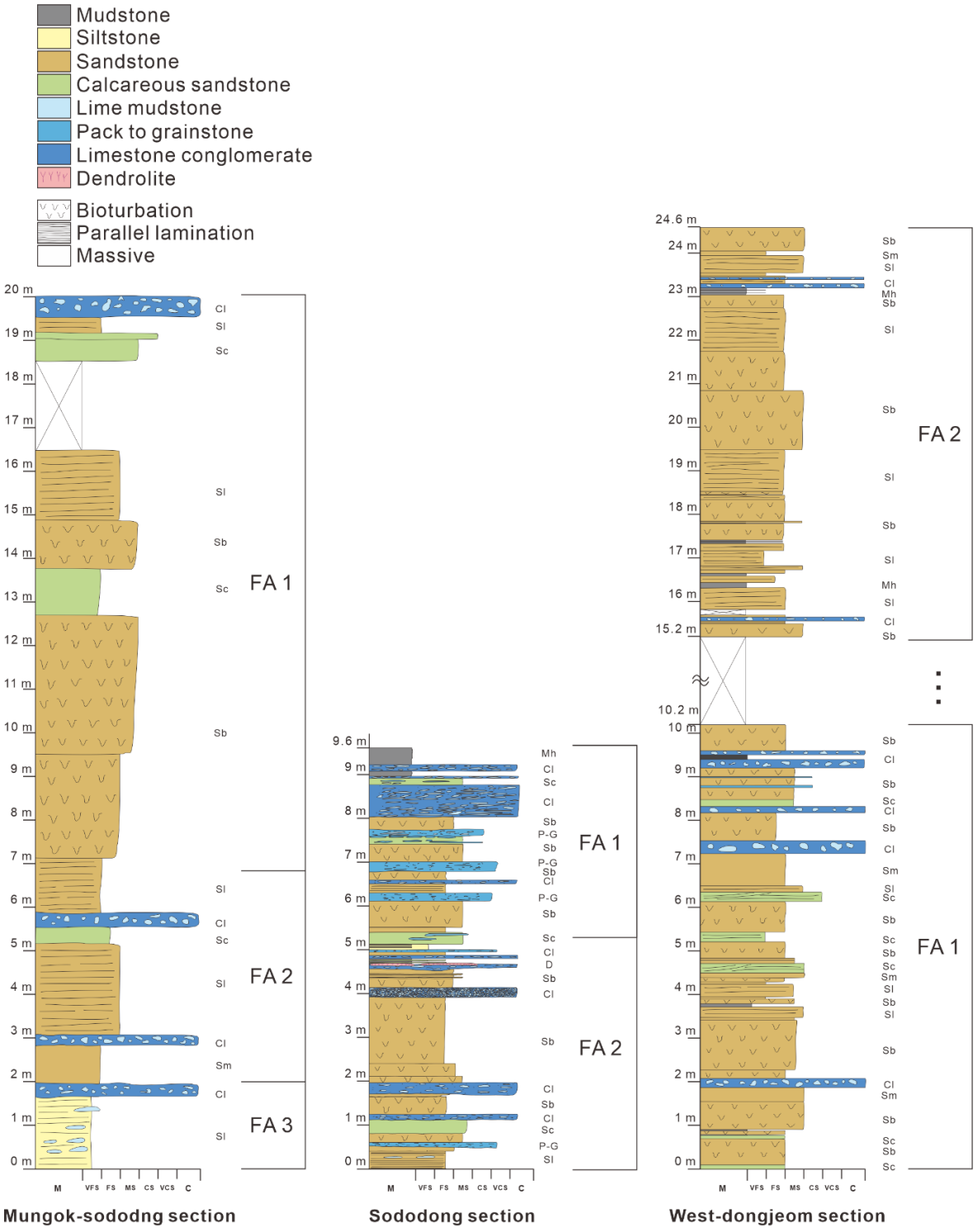

Figure 12. Columnar description of outcrop sections. Sl=Laminated sandstone, Sb=Bioturbated sandstone, Sm=Massive sandstone, Sc=Calcareous sandstone, Mh=Homogeneous mudstone, P-G=Massive pack to grainstone, Clp=Limestone pebble conglomerate.

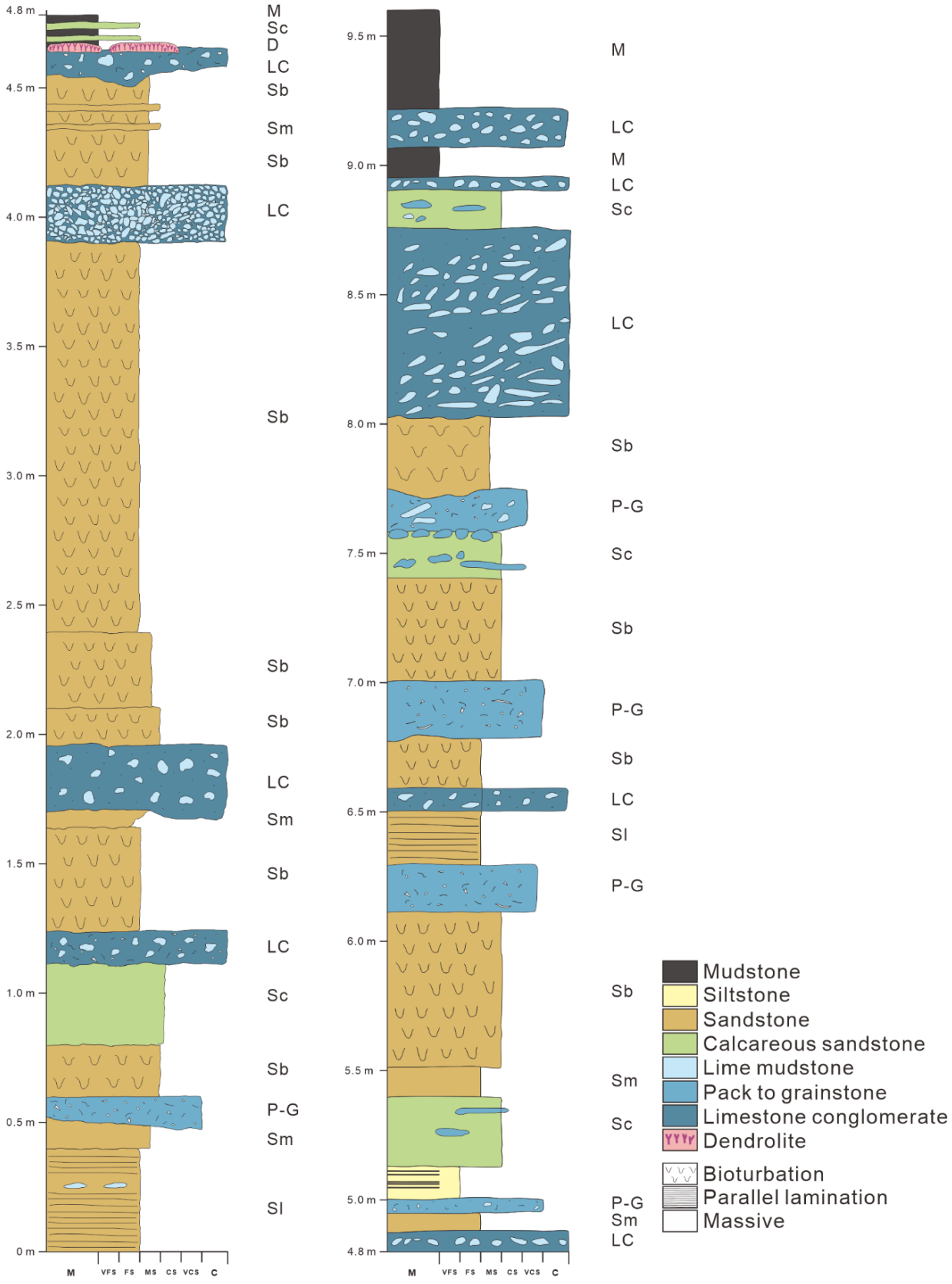

Figure 13. Columnar drawing of the Sododong section with measured thickness of 9.6 m.

6.5. Facies and Facies Associations of Measured Sections

Facies association of measured sections is designated based on detailed observation and comparison of each section. Facies Association 3 occurs in the Mungok-Sododong section and partly in the Sododong section. The Mungok-Sododong section has successive outcrops from the lower Sesong Formation to the middle Sesong Formation. Nodule-bearing shale to siltstone facies is gradually changed into very fine-grained sandstone and fine to medium-grained bioturbated sandstone. The level of bioturbation of the sandstones in the Mungok- Sododong section is variable from BI 1-3. The West-Dongjeom section consists of FA 1 and FA 2. Intensely bioturbated sandstone (BI 3-4) and mudstone interbedded with limestone pebble conglomerate (Fig. 12). The presence of bioturbated sandstone diminishes above the fault, while an alternation of laminated sandstone and homogeneous mudstone becomes apparent. The Hwajeol Formation, characterized by a distinct lithological alternation of limestone and shale, is observed above the laminated sandstone and homogeneous mudstone. The Sododong section is mainly composed of thick, moderately to sparsely bioturbated sandstones and limestone pebble conglomerates that are intercalated within centimeter to decimeter scales. The characteristics of the Sododong section, including a low sedimentation rate represented by the formation of microbialites and the presence of finer grain sizes, are deemed correlative with FA 2 and FA 3.

7. Description of Ichnofabrics and Ichnofacies

The Ichnofacies concept is a valuable approach for identifying distinct sets of trace fossils that reflect particular behaviors of organisms in response to various environmental conditions. (Frey and Seilacher, 1980). Recent comprehensive studies of trace fossils have provided precise information about the depositional environment, including substrate consistency, salinity, turbidity, and paleobathymetry (Frey and Pemberton, 1984; MacEachern *et al.*, 2007). Identifying each ichnogenus of ichnospecies in the core TB-17A was challenging because of the severe disturbances. Instead of identifying ichnogenus and ichnospecies, the ichnological classification was made by measuring the intensity of bioturbation, Bioturbation Index (BI) in the bioturbated sandstones and bioturbated mud to siltstones (Fig. 14). Based on pattern recognition of the primary sedimentary fabric disrupted by biogenic reworking, BI is divided into 1-6 grades (Droser and Bottjer, 1986). BI 1 is designated for the intervals that experienced the least amount of bioturbation; therefore, those intervals have maintained the original sedimentary fabrics. As the sediments are disturbed more extremely by organisms using the substrate for grazing, feeding, or escaping, sedimentary structures are destroyed disorderly, and the recognition of individual biogenic burrows is demanding (BI 5-6) (Fig. 15).

7.1. Horizontal/Subhorizontal Types: A, B

These types of bioturbation show horizontal crawling trails on the surface of soft substrates such as clay and silt. The trails might be isolated in the finer muddy and silty layer or make small troughs following the horizontal axis of the layer. Compared to type A, type B has a larger diameter of the trailing burrow, and burrows are not isolated in the finer layer. Burrows are infilled with sandy substrates and burrow walls or linings are not found in these types are observed in the heterolithic successions and are usually indicating a low degree of bioturbation (BI 1-2).

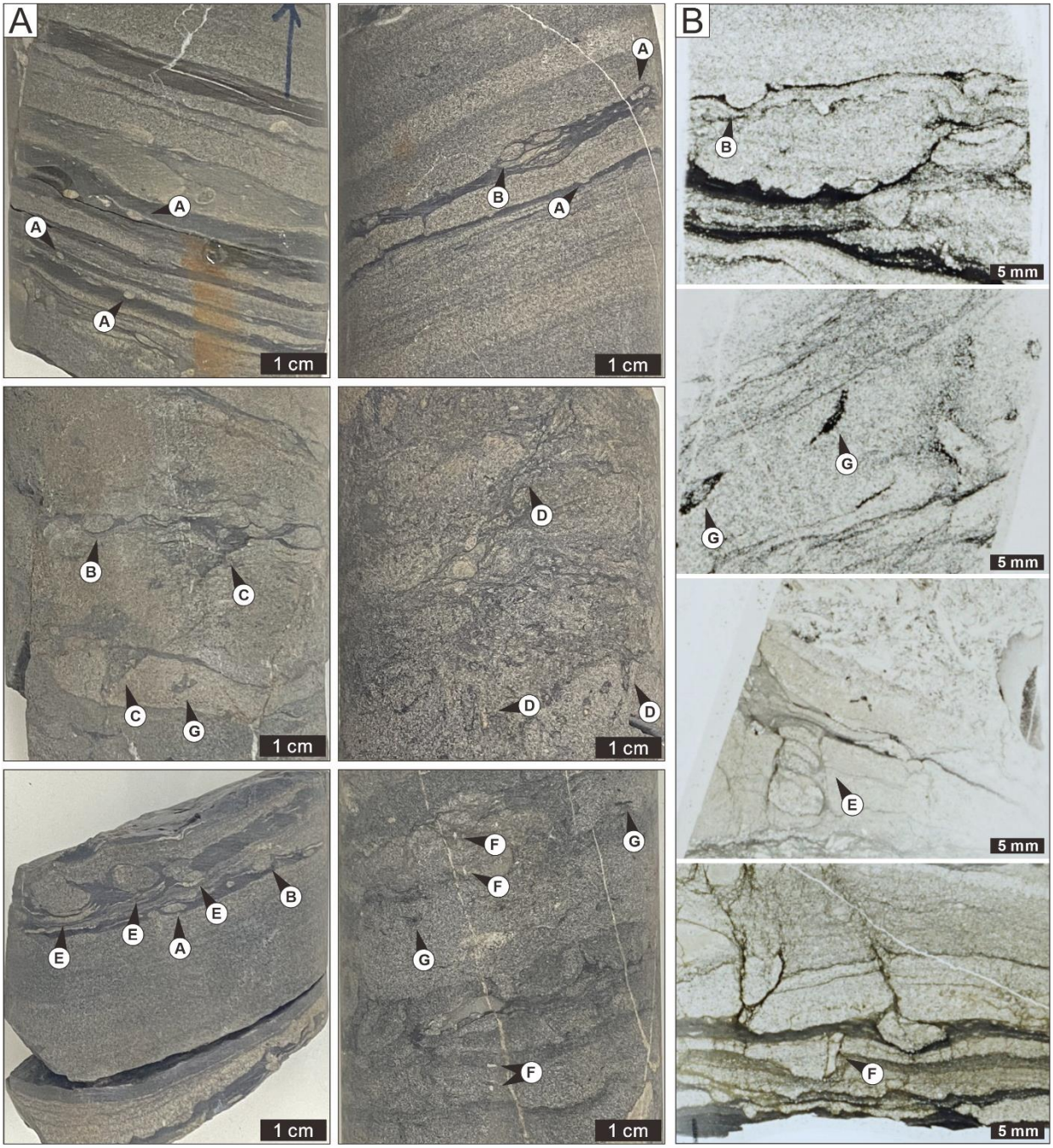

Figure 14. Photograph of seven bioturbation types in the Sesong Formation. (A), (B) Horizontal/subhorizontal type trace fossil of crawling trails within or on soft substrates. (C) Vertical/subvertical type trace fossil characterized by downward tapering shape of burrows. (D) Vertical/subvertical type trace fossil within the calcareous intervals. (E) Vertical/subvertical type trace fossil characterized by spreiten infilling structure. (F), (G) Isolated type trace fossils.

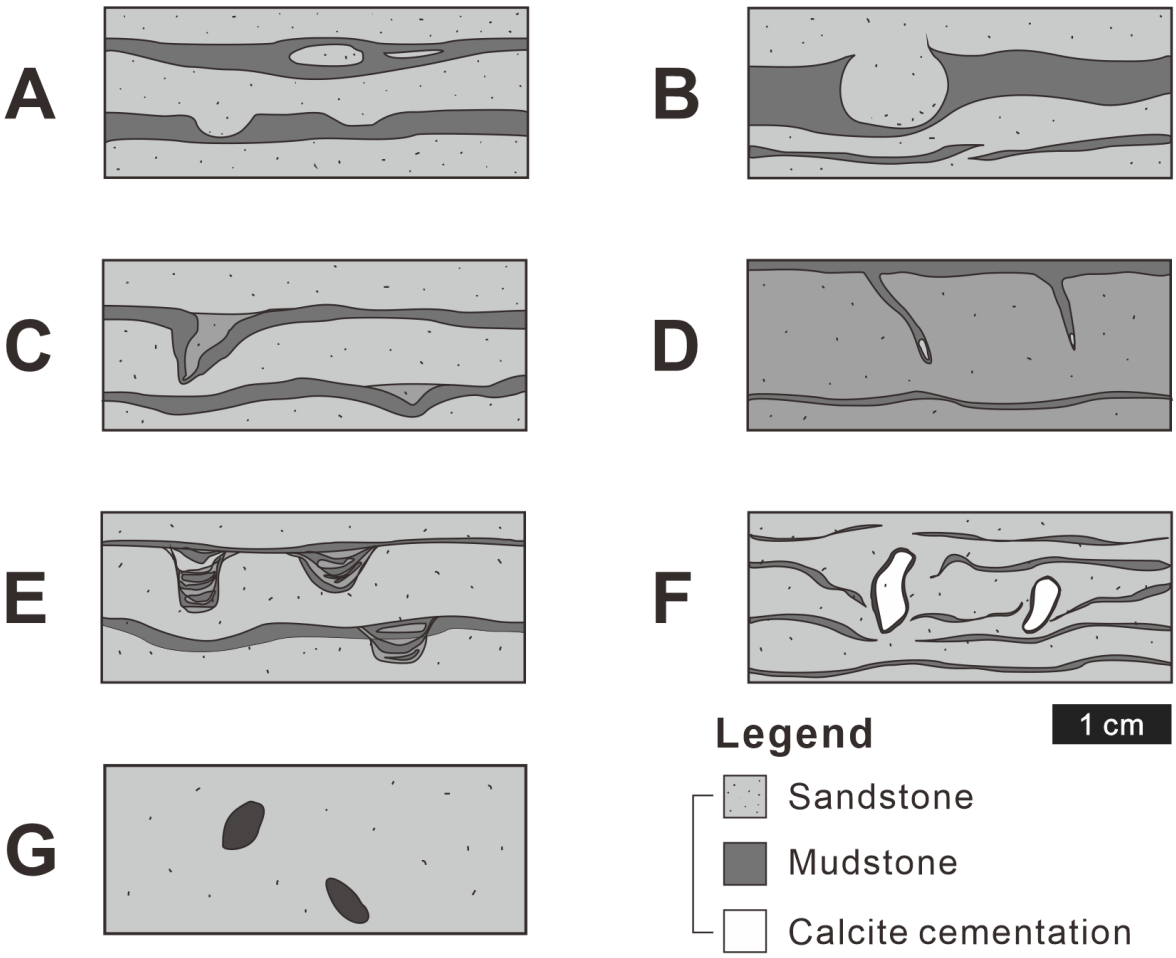

Figure 15. Schematic drawing of bioturbation types.

7.2. Vertical/Subvertical Types: C, D, E

The types have distinctive vertical to subvertical burrows across the layers. The burrows usually start in the muddy layer and are dug into the sandy layer. Type C is characterized by the downward tapering shape of the burrows. The burrows are passively infilled with very fine- to fine-grained quartz sand grains. Burrows found in Type D show a relatively constant and smaller burrow diameter. Type D commonly occurs in calcareous intervals. Burrows of Type E have spreiten infills within them. The infills consist of fine- to medium-grained quartz sand grains, and muddy walls separate the infills. The rate of change in the width of each burrow is smaller than the Type C. Vertical movements of organisms cause a higher rate of sediment mixing than horizontal movements. Therefore, these types of bioturbation are likely to appear in intervals with moderate to high degrees of bioturbation (BI 3-5).

7.3. Isolated Types: F, G

Type F and G are characterized by an unconnected burrowing to the nearby laminations of mudstone. They are found in calcareous sandstone facies. Burrows of Type F show thin, muddy burrow lining and are filled with white-colored calcite cementation. The burrow is elongated following the vertical axis and partly has an angular shape. Type G is represented by dispersed and isolated burrows in calcareous intervals. Burrows of this type have no distinctive inner structures or burrowing walls and are filled with calcareous mud to silt-sized sediments. The surface of the burrows is irregular and unclear in some cases.

8. Description of Dendrolite Bioherm

8.1. Section description

The study area, the Sododong section, is located within the western part of the Hambaeksan fault and the southern part of the Baegunsan syncline in Taebaek City (Fig. 1). The section encompasses the middle part of the formation, exhibiting an exposed thickness of approximately 10 meters (Fig. 13, 16). The lowermost part of the outcrop section is characterized by a continuous reddish limestone conglomerate bed of which the upper boundary (unit boundary 1, UB1) was utilized as a datum for correlation of the overlying beds offset by faults (Fig. 16). The dendrolite bioherm is placed around 4.5-5 m high from the bottom of the measured section. Compared to the other sections within the Sesong Formation, the Sododong section exclusively displays distinct characteristics, notably including slumps within the mixed siliciclastic-carbonate beds and microbial buildups.

The succession primarily comprises the alternating facies of bioturbated sandstone and limestone conglomerate, with minor mudstone and pack-to-grainstone facies (Fig. 13). The bioturbated sandstone beds within the succession are frequently intercalated with layers of silt to mudstone. The grain size of the sandstone beds varies from very fine-grained sandstone to medium-grained sandstone, and they exhibit sparse to moderate bioturbation. The bioturbated sandstone beds occasionally have a sharp and erosive upper boundary. The decimeter scale of alternation bioturbated sandstone and limestone conglomerate is evident within the weathered surfaces. Microbial buildups are found in or rest on the limestone conglomerate beds.

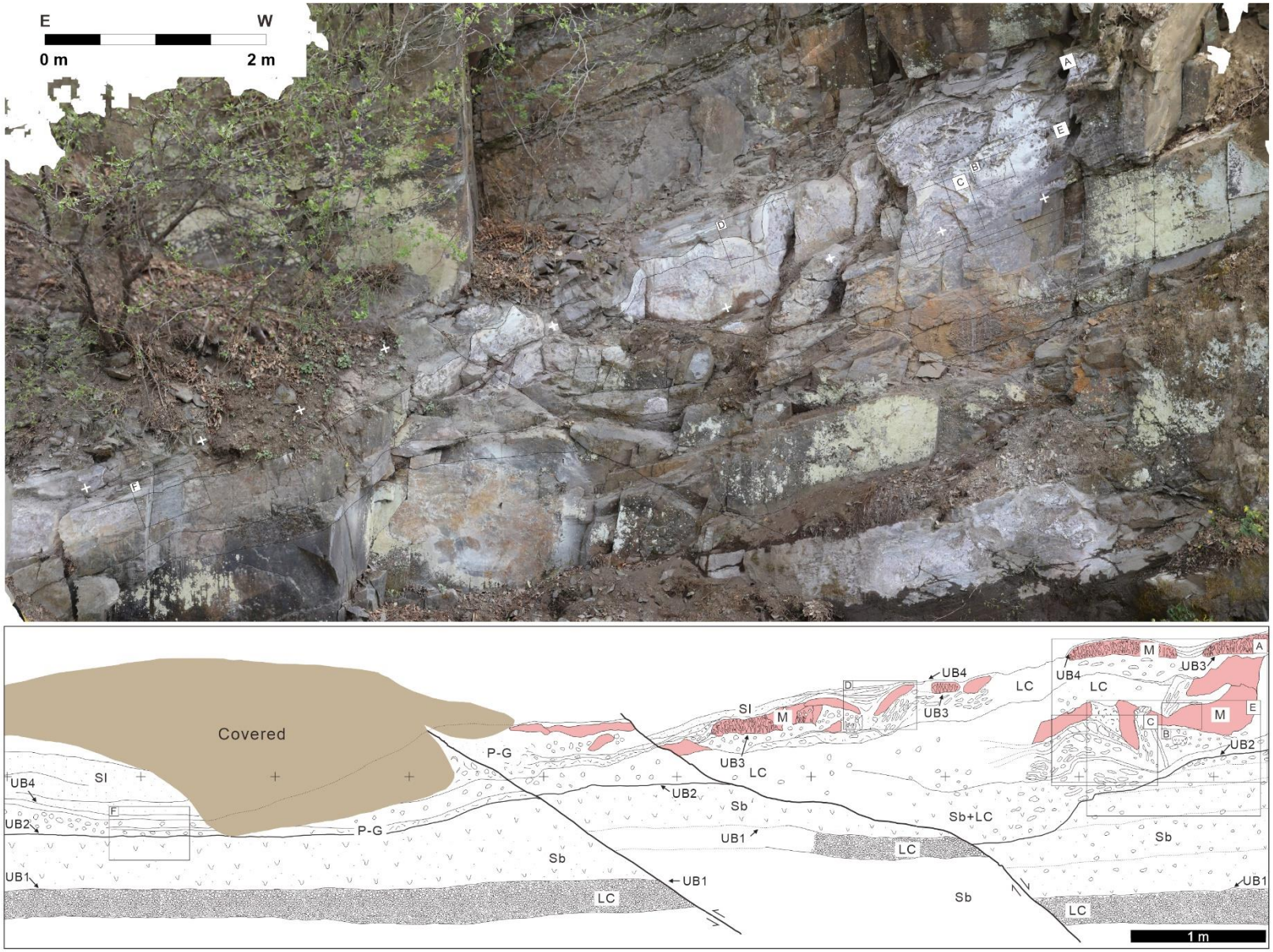

Figure 16. Photograph and field sketch of the outcrop of Sododong section.

8.2. Sedimentary structures/deformation structure of limestone conglomerate

The lowermost limestone conglomerate consists of well-sorted small-pebble-grade reddish lime mudstone clasts. The overlying strata are represented by medium-bedded bioturbated sandstone with rarely distributed limestone clasts. It is overlain by a disorganized limestone conglomerate bed overlain by the dendrolite bioherms (Fig. 17A). The lower boundary of the disorganized limestone conglomerate (UB2) exhibits a notable erosional surface which is laterally traceable almost 10 m with maximum relief reaching approximately 70 cm. The surface continuously slopes eastward. The disorganized bed is characterized by a chaotic mixture of different materials, such as blocks of microbialites, lime mudstone clasts, skeletal grains, sandy matrix, and fine-siliciclastic matrix (Fig. 17B). Some part of the disorganized bed is represented by alternating beds of limestone conglomerate layers and bioturbated sandstone layers, which buckled together (Fig. 17C, D). The buckled layers show folded geometry with steep down-slope and gentle up-slope limbs (Fig. 17D). The long axis of limestone clasts in the limestone conglomerate is aligned with the deformed bedding plane. Large aphanitic microbialite blocks tend to elongate following this bedding as well. The limestone conglomerate beds are partly brecciated in situ and rotated, forming narrow gaps between brecciated blocks, which are filled with gray-colored siliciclastic matrix (Fig. 17C, 18A-D). Certain bioturbated sandstone laminas within the limestone conglomerate beds exist with low continuity. The thickness of the bioturbated sandstone underlying the disorganized limestone conglomerate varies from approximately 1.5 meters to 0.8 meters eastward direction (Fig. 16 and 17E) as well as the thickness of the correlative bed of the limestone conglomerate progressively diminishes (Fig. 17F).

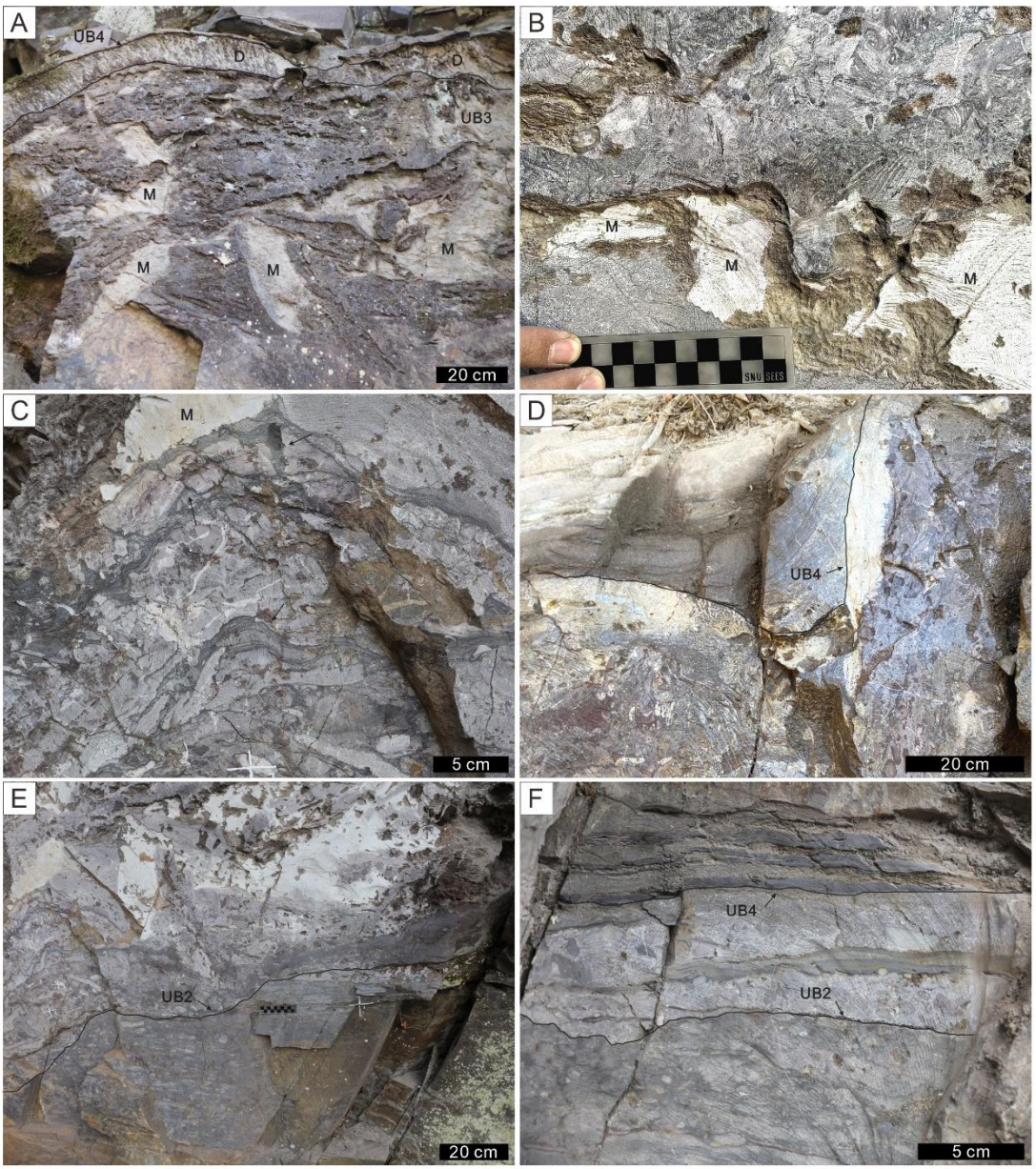

Figure 17. Detailed photographs of Figure 15. Unit boundaries (UB1-4) are marked on the photographs. (A) Disorganized limestone conglomerate-microbialite bed and overlying dendrolite bioherms. (B) Detailed view of the disorganized bed consisting of limestone clasts, sandy and muddy matrix, and microbialites. (C) Brecciatied limestone block and laminated sandstone. Lamina in the sandstone bent around limestone blocks and infiltrate into the interspaces between blocks. (D) Rotated block of limestone conglomerate. (E) Erosive boundary between bioturbated sandstone and disorganized bed. (F) The disorganized bed thins eastward to form limestone conglomerate and intervening sandstone layer. The basal erosional boundary (UB2) and the uppermost boundary (UB4) are marked.

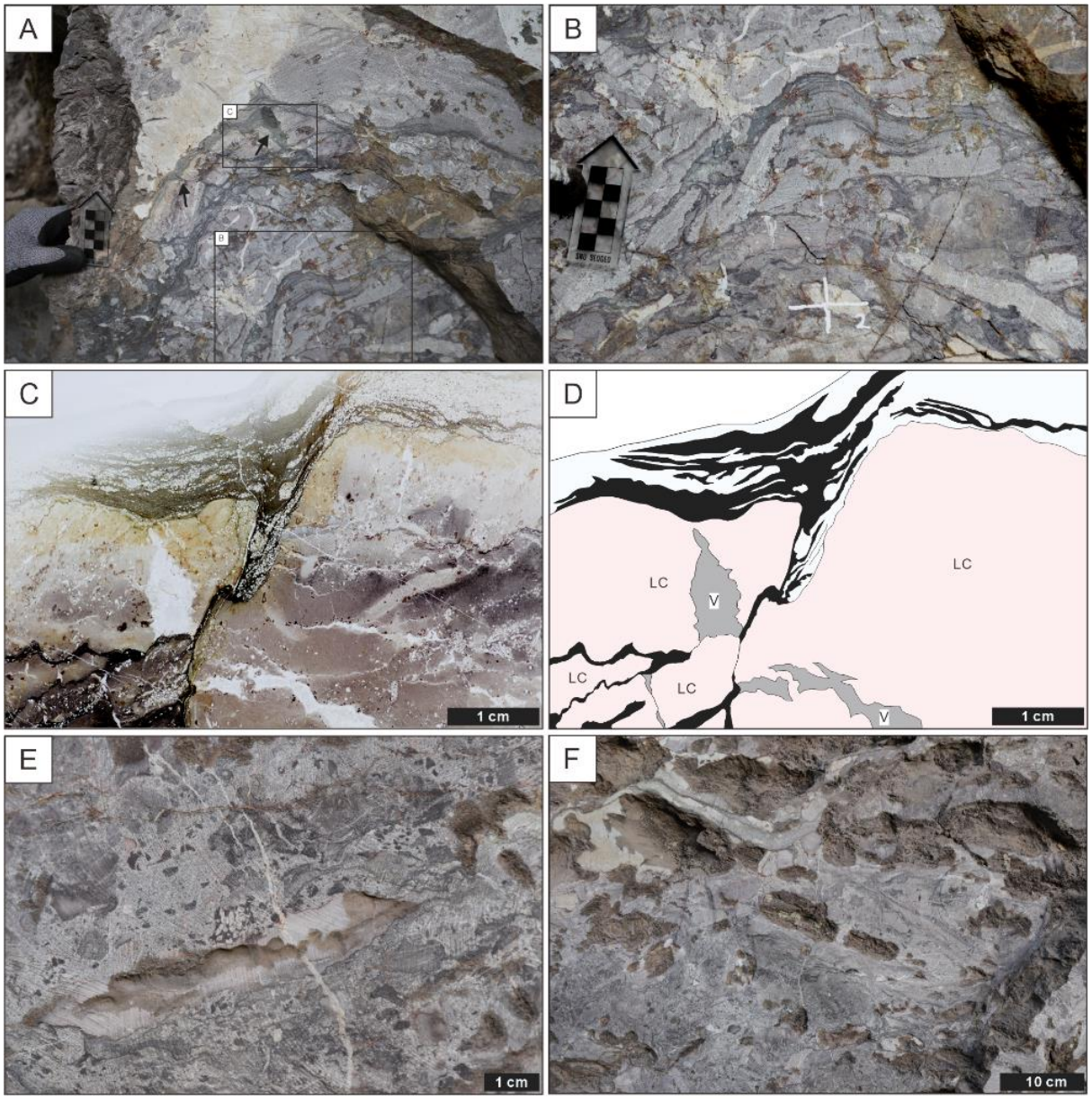

Figure 18. Photographs of limestone conglomerate. (A) Brecciated limestone blocks. The interspace between the limestone blocks is infiltrated by sandstone (black arrows). (B) Soft sediment deformation structure of the sandstone. (C) Photograph of thin section on marked location on (A). (D) Line drawing of (C) showing sandstone infiltrated into the gap. LC: limestone clast, Sb: bioturbated sandstone, Mb: bioturbated mudstone, V: calcite vein. (E) Bioturbated sandstone forming the matrix part of the disorganized bed. Burrows of bioturbated sandstone are dislocated but the original shape is retained. (F) Soft sediment deformation structure of bioturbated sandstone. Folding due to ductile deformation is marked as dotted lines.

8.3. Description of the dendrolite bioherms

The disorganized limestone conglomerate bed is bounded above by a sharp, smooth surface (UB3), which can be traced in most outcrops except the leftmost part, where the deformation structure is not evident (Fig. 17A). The layering in the underlying bed usually ends against this surface, and many limestone clasts were cut sharply by this surface (Fig. 19A, 20A). The dendrolite bioherms occur on top of this surface, with an exposed width and height of 50 cm and 20 cm, respectively (Fig. 17A). The continuity of these bioherms is low, and their distribution is confined solely to the limestone conglomerate intercalated within the sandstone. Accretionary growth of clotted, non-dendritic microbialites is occasionally present at the side surfaces of the dendrolite organic buildups (Fig. 19A, D). The dendrolite consists of dendroids that branch upward, taper downward, and admixture of bioclastic limestone conglomerate matrices and quartz (Fig. 20). The size of dendroids is variable, ranging from 20 mm to 35 mm. The dendroids comprise biogenic microclots and micrites filling the interspaces (Fig. 20). Due to the recrystallization of the calcite that forms the dendroids, their specific microstructures are hardly recognizable. The matrices of the dendrolite comprised diverse constituents, including skeletal grains, quartz grains, intraclasts of lime mudstone, and microbialites such as stromatolites (Fig. 20B-E). The dendrolite bioherms primarily consist of bioclast derived from brachiopod shells, which display preserved original form in the uppermost part (Fig. 20A, B). The dendrolite bioherms are overlain by a thin layer of greenish clay minerals (Fig.19C) on unit boundary 4 (UB4).

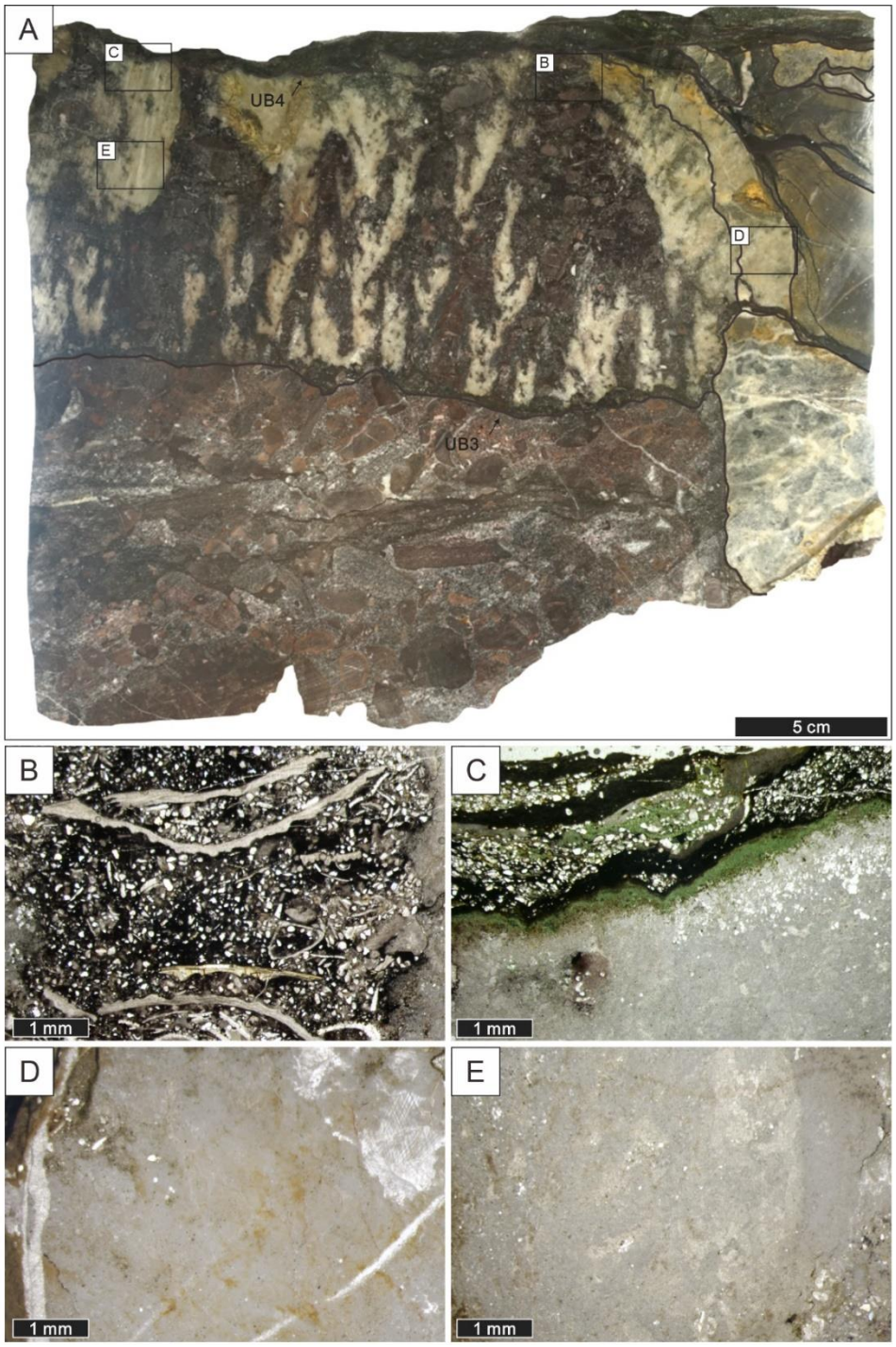

Figure 19. (A) Photograph of a slab of dendrolite bioherm showing the lower and the upper boundaries. Note branching upward and upward widening microbial community forming dendroids. It also shows lateral margin of the bioherm characterized by laterally accreted aphanitic microbialite. (B) Well-preserved skeletal grains in the upper portion of dendrolite. (C) Layer of greenish clay mineral on the upper surface of the dendrolite. (D) Photomicrograph of clotted microbialite, and (E) dendrolite.

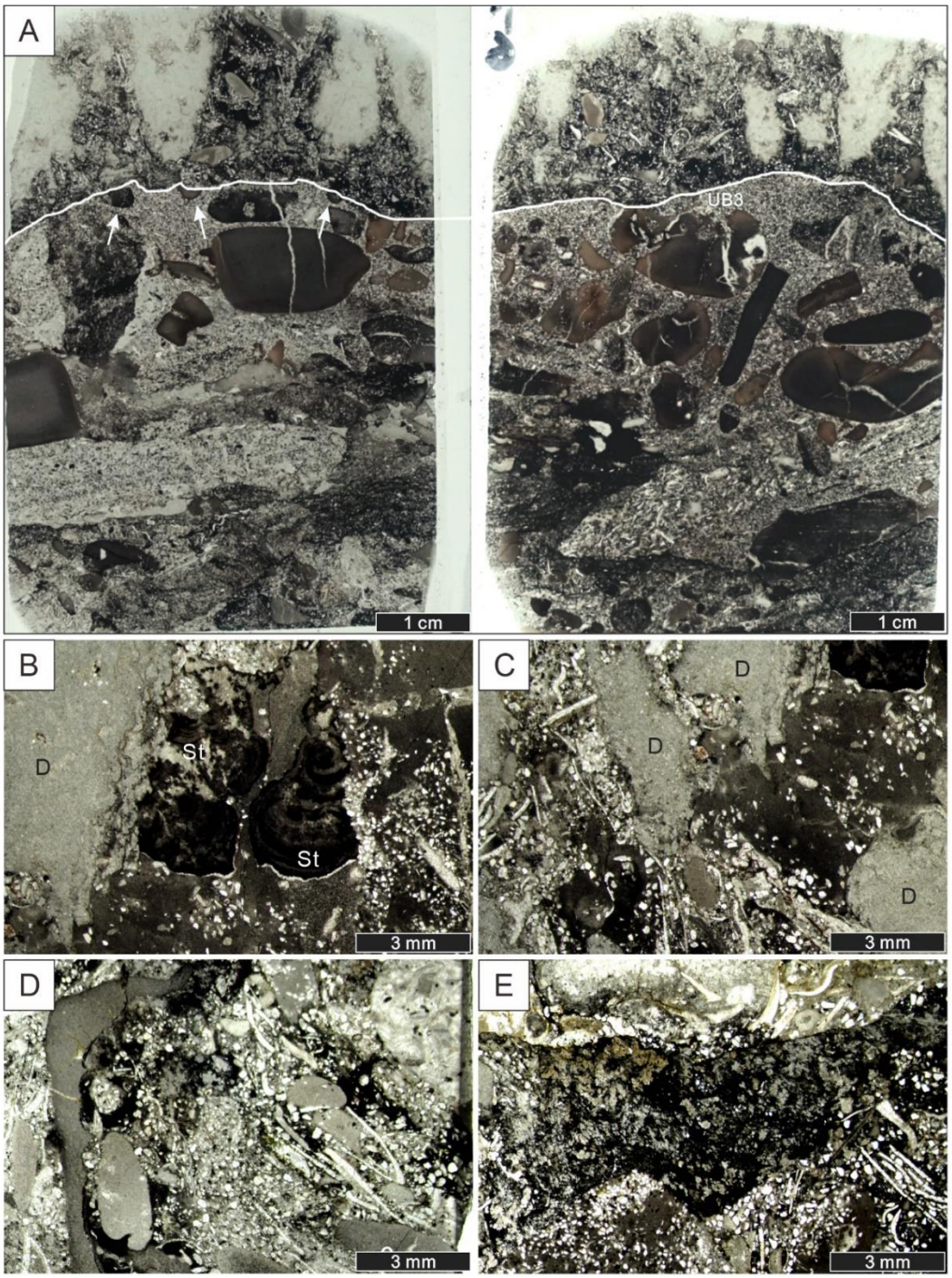

Figure 20. Photomicrographs of hardground surface and matrices of dendrolite. (A) Hardground surface (UB3). Eroded lime mudstone clasts are marked with white arrows. (B) Stromatolite intraclasts. (C) Micrite (dark gray) filling the space between dendroids (light gray). (D) Detrital grains within dendrolite, including lime mudstone intraclasts, skeletal grains, and quartz grains. (E) Microbialite intraclasts in the matrix of dendrolite.

9. Formative process of limestone conglomerate-microbialite bed

Deformation structures in the disorganized limestone conglomerate demonstrate material deformation with rigid bodies and soft matrices. Rigid bodies, such as microbialite blocks and limestone clasts in the disorganized bed, are those influenced by early carbonate cementation (Demicco and Hardie, 1994). The matrix around the rigid bodies is mostly unconsolidated sediment of sand and mud. Wholesale buckling of conglomerate and sandstone alternation beds is indicative of ductile deformation of original horizontal beds (Fig. 21F). Well-preserved lamination and bioturbation structures in the sandstone layers suggest that the sandstone grains have not been disaggregated during deformation, and the dislocation of the framework structure was minimal. The rigid limestone clasts within the conglomerate bed showed little to no influence from brittle deformation except for a few instances. Long limestone clasts near the axial part of the folding are in-situ brecciated, and the boundaries slip as a form of a normal fault, indicating extensional stress. The lamination of mudstone and sandstone bent around the limestone blocks and infiltrated into the narrow gaps formed by the brittle deformation of the rigid body. The injection is ascribed to the high fluid pressure of the deforming material, induced by the omnipresence of rigid bodies, which hampers free dissipation of the pore pressure (Chen and Lee, 2013). Such high pore pressure provided a supporting mechanism for the clasts within the matrix, resulting in ductile deformation of the clast-rich limestone conglomerate bed (Myrow et al., 2004). The direction of fold axis inclination of the asymmetrically folded strata indicates that there most likely was shear stress causing eastward movement of the mass. The direction is consistent with the direction of a slope represented by the sharp erosional boundary (UB2) underneath the disorganized bed. These lines of evidence point toward slumping as a mechanism for the deformation of the original strata.

The upper surface of the slumped mass probably was rough with significant relief

(Martinez et al., 2005). The sharp erosional upper boundary, knife-cutting clasts included in the underlying slumped mass, is interpreted as hardground surface, which resulted from early cementation of the seafloor and abrasion of the surface by waves and currents. As the substrate is stabilized, microbial communities start inhabiting the hardground surface not in continuous mats or film but discrete globules with detrital grains of bioclasts, intraclasts, and quartz sands. It resulted in the dendrolite mesostructure of the branching microbial masses intermixed with grains supplied by gentle currents and waves. The general energy level of these transportation mechanisms was, most likely, strong enough to carry these grains but insufficient to sweep away the sediment grains baffled within meadows of dendroids. Aphanitic microbialite accreted on the girdles of the dendrolite bioherms represents a separate depositional stage with less supply of detrital sediments. The microbialites were mantled by thin beds of greenish mudstone and sandstone, which terminated the growth of dendrolite by increased turbidity and burial of the growth surface.

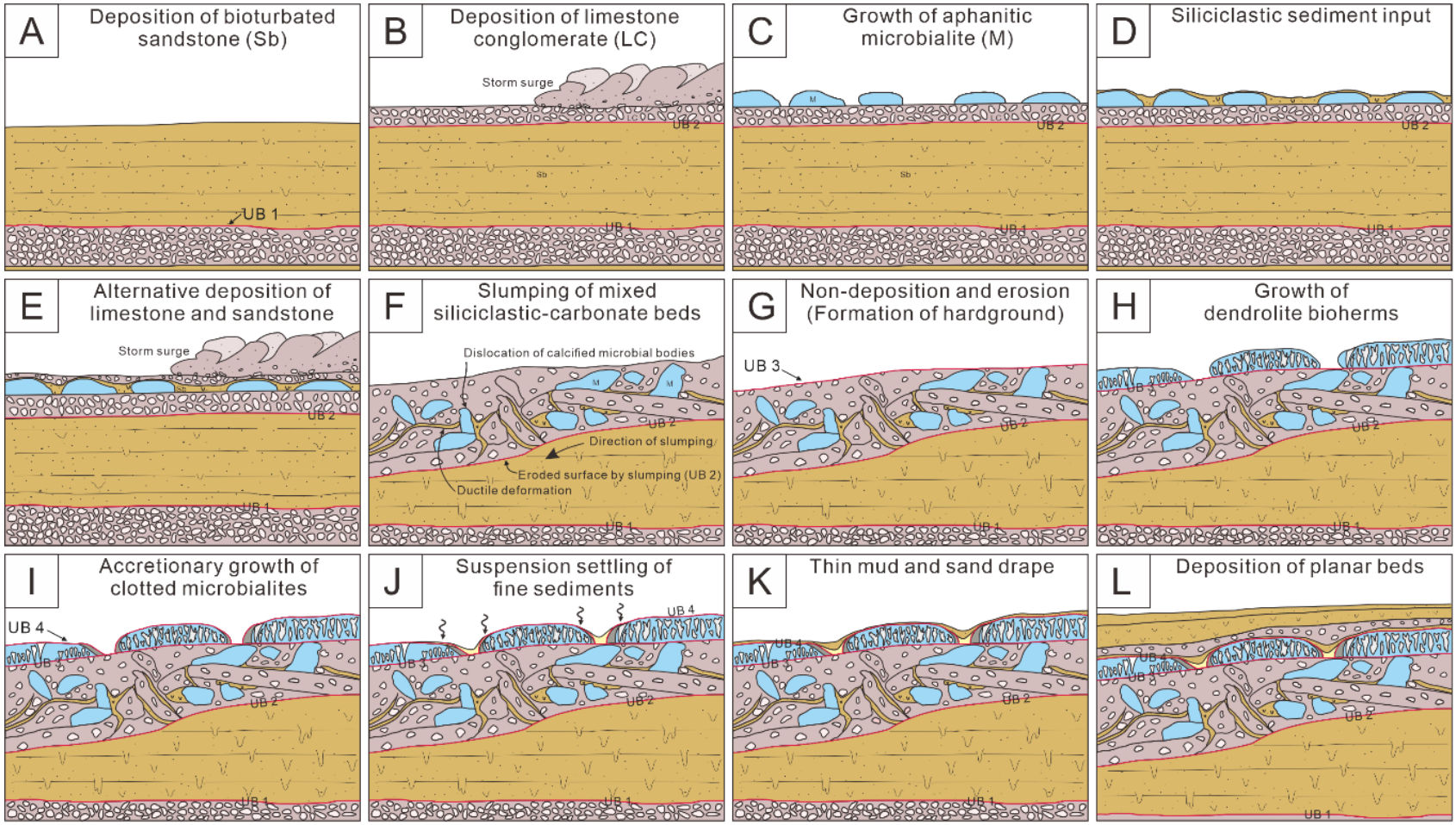

Figure 21. Schematic model of formative processes of the disorganized bed and dendrolite. See the text for a detailed explanation.

10. Discussion

10.1. Depositional environments

The Sesong Formation can be divided into four members: 1) the basal member consists of shale with lime mudstone nodules and limestone conglomerate, 2) the lower member characterized by shale dominant lithology with intercalated thin fine sandstone beds, 3) the middle member characterized by bioturbated sandstone facies, and 4) the upper member is represented by sandstone beds finer than middle member, with an upward fining trend (Park et al., 2012). This upward fining trend gradually changes into a limestone-shale couplet facies of the overlying Hwajeol Formation. Specifically, the upper half of the lower member, middle and upper members can be discretely divided into three facies associations that exhibit variations in their respective depositional environments.

The basal member, the lowermost Sesong Formation, is characterized by prominent shale facies that conspicuously overlies the drowning surface of the topmost Daegi Formation, supporting the interpretation of an abrupt transgression occurring at the boundary (Kwon et al., 2006). The basal member consisting of shale facies is widely interpreted as representing the maximum depth of the depositional environment within the formation. (Joo and Ryu, 2012; Lim et al., 2015). The rise of the relative sea level caused a notable transformation of the depositional modes from shallow subtidal carbonate deposition in an open marine environment to a more tranquil, deeper deposition of clastic sediments (Kwon et al., 2006; Zeller et al., 2015).

The gradual decrease in the proportion of shale-dominated facies and simultaneous increase of sand-dominated facies indicates an increment in the siliciclastic sediment supply, signifying a shift in the depositional environment from a low-energy offshore environment to a relatively higher-energy offshore transition zone below the fair weather wave base (Fig. 21). The change was gradual across the

middle part of the lower member where thin sandstone layers start to occur. *Cruziana*-type ichnofacies (*Teichichnus* and *Planolites*) suggests the presence of tranquil aquatic environments beneath the fair-weather wave base (Pemberton et al., 1992). Fine sandstone-dominated FA3 changes upward into coarser FA2, and the grain size culminates in FA1 with medium sandstone (Fig. 11). The degree of bioturbation and diversity of burrow types also gradually increase upward from FA1 to FA3 (Fig. 11 and 22). These changes indicate gradual shallowing, which may result from slow progradation of the system (Tucker, 2003; Zeller et al., 2015). The following succession of facies associations 2 and 3 represent continuing transgression.

The facies associations of the Sesong Formation suggest that it formed in the offshore transition zone, between fair-weather and storm wave bases (*sensu* Galloway and Hobday, 1996). Now widely recognized as a main subdivision of the beach-to-offshore profile, it had been regarded as lower shoreface to offshore (Joo and Ryu, 2012) and outer shelf (Choi et al., 2004; Kwon et al., 2006). Considering steeper shoreface slope angle and average fair weather and storm wave base depth of 10-20 m and 80-100 m, respectively, the proportion of the offshore transition on the shallow ramp-type platform is significant. Many meter-scale cycles formed on this type of platform consist only of offshore transition facies (e.g., Kwon et al., 2006; Cho and Hong, 2021). In this regard, refining the facies belts of the offshore transition is important.

The appearance of laminated sandstone facies, generally finer than bioturbated sandstone facies in the upper part of the formation, indicates the increase in relative sea level. The decreased bioturbation index, accompanied by variations in grain size,

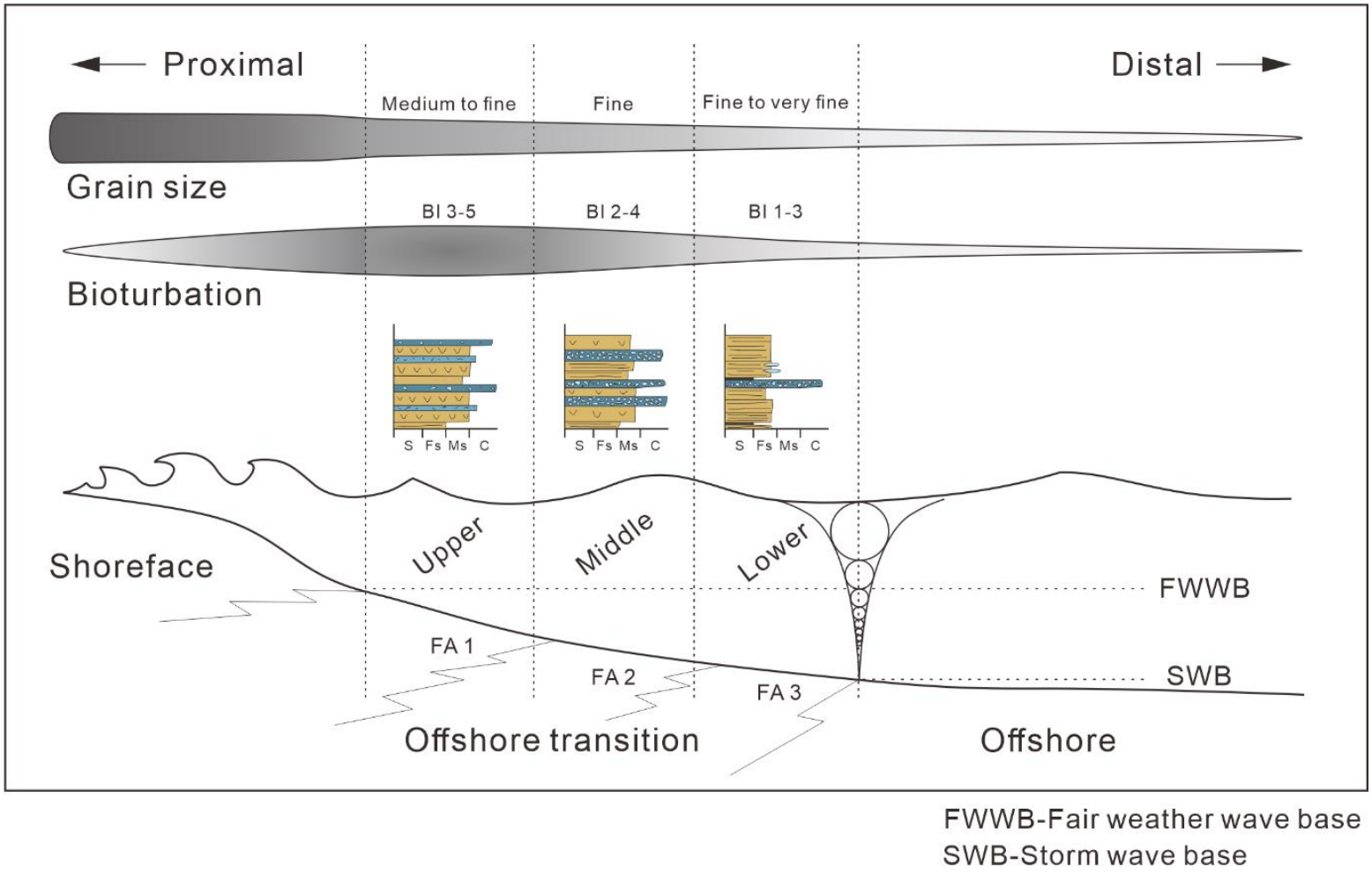

Figure 22. Facies associations of the upper part of the Sesong Formation presented with depth of fair-weather wave base and storm wave base. Schematic grain size and bioturbation index variation from shoreface (proximal part) to offshore (distal part), which can be used as criteria for subdivision of offshore transition zone.

reflects the environmental constraints exerted on organisms due to increased water depth (Seilacher et al., 2005; Bromley, 2012).

Consequently, the activity of sediment-dwelling organisms exhibited a decline, corresponding to the relative sea-level rise, which results in a slightly deeper depositional environment. A consistent deepening pattern is observed on the uppermost part of the Sesong Formation, transitioning towards a deeper subtidal depositional condition. This marks the initiation of sedimentation for the limestone-shale couplet facies comprising the Hwajeol Formation.

10.2. Triggering mechanism of the slump

Numerous hypotheses have been proposed to explain the triggering mechanisms of slumps. These hypotheses encompass seismic shakings such as earthquakes (Seed, 1979; Obermeier, 1996), actions of waves and storms (Bjerrum, 1973; Nataraja and Gill, 1983), fluctuation of groundwater (Jeyapalan et al., 1983; Li et al., 1996), relative sea-level fall (Chen et al., 2011), and sediment overloading by rapid sedimentation (Anketell et al., 1970). The triggering mechanism for the slump in this study is postulated to be powerful wave actions generated by storms (Watts et al., 2005; Shanmugam, 2010). Undoubtedly, seismic activity is the most prevalent triggering factor for sediment liquefaction and fluidization (Seed, 1979). Nevertheless, the preservation of the inherent parallel lamination in the strata located both above and below the limestone conglomerate-microbialite bed proves that the deformation structure within the Sesong Formation did not arise from seismic shaking. Rather than being attributed to seismic activity, the deformation structure within the Sesong Formation can be ascribed to the cyclic loading exerted by storms, which subject to the sediments positioned on the slope to shear stress, resulting in the instability of unconsolidated sediments. As a result, the instability of sediments results in mass

transportation, such as slides and slumps. The slumping event occurred within the upslope region from the head scar, causing the transportation of sediments in a downslope direction and resulting in the formation of asymmetric-fold-like deformation structures within the sediments downstream (Fig. 23). The slumping of the limestone conglomerate made a confined slump scar on the underlying bioturbated sandstone bed. The deformed bed is located within the lower part of the middle member of the Sesong Formation and exhibits an extension of less than a few meters (Fig. 16).

10.3. Hardground surface

Hardgrounds are centimeter-sized discontinuous surfaces of synsedimentary lithification, having existed as hardened sea floors before the deposition of the overlying sediment (Flügel, 2010). Hardground surfaces are common in various Cambrian marine sedimentological records (Glumac and Walker, 2002; Kruse and Zhuravlev, 2008; Alvaro and Clausen, 2010; Zamora et al., 2010). It signifies a surface characterized by increased lithification or consolidation compared to the surrounding sedimentary layers. Multiple processes can potentially induce non-deposition and the subsequent formation of hardgrounds: drowning resulting from relative sea-level rise, dissolution of carbonates and silica at the seabed, and intermittent scouring caused by bottom currents (Tucker and Wright, 2009; Flügel, 2010). The combination of a distinct erosional upper boundary and the presence of erosive lime mudstone clasts within the underlying slumped mass is interpreted as evidence of a hardground surface. This hardground experienced abrasion resulting from the combined effects of wave action and the influence of ocean currents during periods of relative sea-level rise.

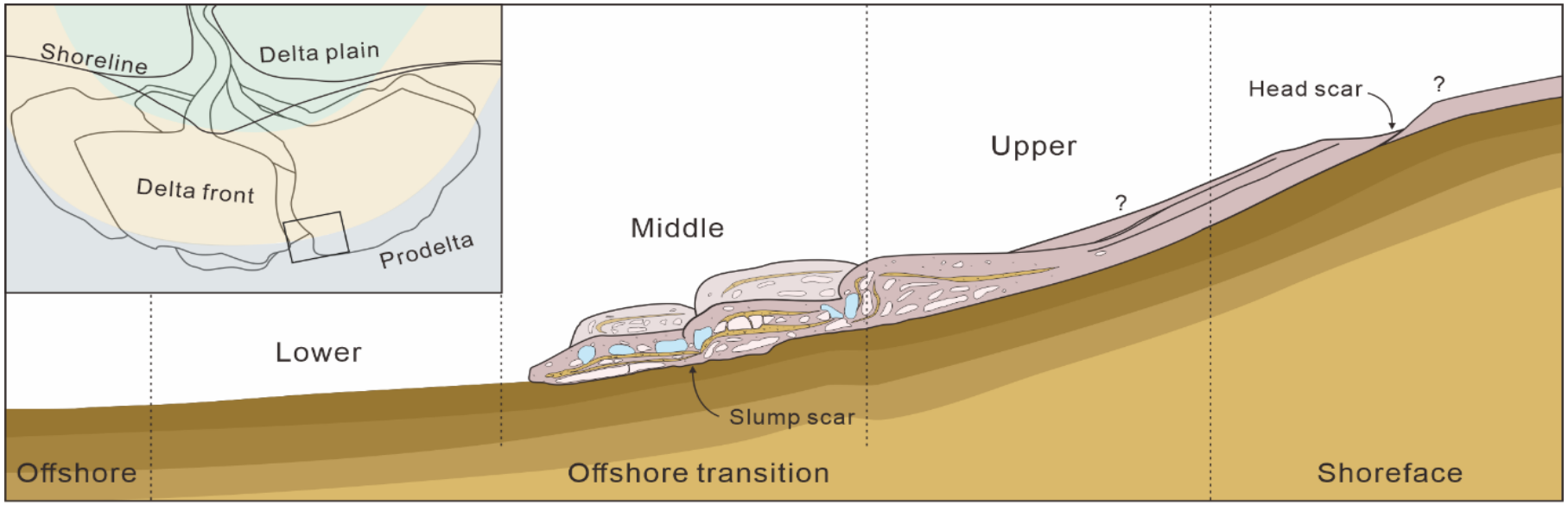

Figure 23. Slumping in the offshore transition zone which is linked with probable deltaic system.

10.4. Deltaic system

Mixed siliciclastic carbonate platform receives siliciclastic sediment from the hinterland via transitional depositional environments such as deltas (e.g., Braga et al., 2001; Lee and Chough, 2011; Pujalte et al., 2016). Sandy sediments from siliciclastic units of the Tabaeksan Basin transported most likely through deltaic system although the direct evidence of the delta (cf., Lee and Chough, 2011). Laterally discontinuous sandstone units of the Sesong Formation with shallow marine sedimentary features (Kobayashi, 1935; Cheong et al., 1969; Choi et al., 1998; Choi et al., 2004) might reflect lobate geometry of the deltaic systems. The decrease in sediment supply and sediment starvation without major water-depth change suggest that there might be laterally heterogeneous sedimentary system and resulting facies distribution suggests potential existence of laterally switching delta lobes within the Sesong Formation. The offshore area, which corresponds to the prodelta region within the deltaic system, demonstrates a bathymetric nature characterized by a relatively gentle slope degree of only a few degrees or less. Within this relatively flat geometric area, mass transportation phenomena such as slides and slumps are considerably hindered. However, the existence of a deltaic system generally indicated a more pronounced slope inclination due to the presence of delta lobes. The heightened slope inclination leads to increased instability and the potential for slumping. Furthermore, in the event of a delta lobe switching, the previous lobe may become abandoned, leading to sediment starvation within that particular area. The decrease in sediment input leads to the formation of hardground surfaces and microbialites.

10.5. Correlation with other North China Platform

The studied section is correlated with the lower part of the upper Sesong Formation based on stratigraphic position, the transition of facies association from FA2 to FA1,

and carbon isotope values compared with those from other sections. A stable carbon isotope excursion was reported in the correlated interval, which, in turn, correlated with the global isotopic event, known as Steptoean positive isotopic carbon excursion (SPICE). SPICE in the North China Platform was compared between Shandong and Taebaek areas (Chen et al., 2012). The excursion occurs in the upper part of the Gushan Formation and is characterized by deformed strata and overlying microbial bioherms (Chen et al., 2011). The deformed bed consists of soft-sediment deformation structures such as clastic dykes, lime mudstone breccias, and homogenized oolite, which were generated by liquefaction/fluidization and upward escape of fluid (Chen et al., 2011). Sea-level lowering and associated non-equilibrium between hydrostatic pressure and pore-water pressure were ascribed to the triggering mechanism of the deformation (Hilbrechet, 1989; Chen et al., 2011). The extensive erosional surface on top of this deformed bed was made during subaerial platform exposure.

The appearance of the deformed bed, erosional boundary, and microbialite growth has certain similarity. But the mode of deposition in the Sesong Formation is different in that the deformation took place with lateral, down-slope movement, that the disaggregation of the matrix material was very limited, that the erosional surface was made under seawater, and that the buried by deeper facies during subsequent transgression. These interpretations collectively suggest that there might have been a significant slope in the Taebaeksan Basin during the Sesong deposition. The dominance of sandstone facies in the upper part of the Sesong Formation is most likely supplied through a certain type of deltaic system to the offshore transitional zone, which is comparable to prodelta. The slope of the delta front is usually around 1-2 degrees but can reach up to 23 degrees at the head of the slope (Lutermauer and Finn, 1983). Global sea-level lowering and associated exposure of the hinterland area of the Taebaeksan Basin might result in the extension of the fluvial system in the hinterland to the platform

interior. The lowered sea level also gave rise to the non-equilibrium in pore-water and hydrostatic pressure, which made the sediments more sensitive to physical perturbation (Chen et al., 2011). The combination of global sea-level lowering and deltaic slope development and the resultant disorganized bed demonstrates that the global environmental event can be represented differently in a single platform.

11. Conclusions and summary

The Sesong Formation, a constituent formation of the Taebaek Group within the Taebaeksan Basin, can be divided into two main parts: the lower part dominated by shale and the upper part composed of sandstone. Within the upper part of the Sesong Formation, there are eight distinct sedimentary facies: homogeneous mudstone (Facies Mh), bioturbated mud to siltstone (Facies Mb), laminated sandstone (Facies Sl), bioturbated sandstone (Facies Sb), massive sandstone (Facies Sm), calcareous sandstone (Facies Sc), massive pack to grainstone (Facies P-G), and limestone pebble conglomerate (Facies Clp). These eight sedimentary facies can be further categorized into three facies associations. Facies Association 1 (FA1) is characterized by bioturbated sandstone with grain size ranging from fine to medium sand and a pronounced degree of bioturbation index (BI 3-5). The *Cruziana*-type ichnofacies, including *Teichichnus* and *Planolites*, indicate tranquil aquatic environments below the fair-weather wave base. FA1 represents deposition in the proximal region of the offshore transition zone. Facies Association 2 (FA2) consists primarily of bioturbated sandstone with a reduced level of bioturbation index and a greater proportion of intercalated mudstone. On the other hand, Facies Association 3 (FA3) is characterized by fine-grained laminated sandstone and mudstone facies that lacks bioturbation, which implies most distal facies association among the others. After the sedimentation of the lower part of the Sesong Formation, subsequent shallowing resulted in the deposition of the coarser units primarily comprised of FA1. The following rise in sea level led to the development of facies succession from FA2 to FA3 in the upper part of the formation. Subsequently, rising sea levels led to the deposition of lime mudstone and mudstone alternation of the Hwajeol Formation.

A prominent feature of deformation structures and microbialites occurs in the Sododong section. The lower portion of the section consists of fine-grained bioturbated

sandstone, laminated sandstone, and limestone conglomerate, indicative of the middle offshore transition (FA2). The upper portion is composed of medium- to fine-grained bioturbated sandstone, calcareous sandstone containing pack-to-grainstone clasts, frequent intercalations of bioclastic pack to grainstone, and limestone conglomerate, associated with the upper offshore transition (FA1). The irregularly shaped microbial intraclasts and bioturbated sandstone within the disorganized limestone conglomerate beds originated from complex sedimentary and deformational processes. Brecciation and rotation of the limestone conglomerate beds are evident, with interstitial spaces filled by bioturbated sandstone resulting from injected unconsolidated sandstones. The limited degree of lateral movement, restricted disaggregation of grains, and localized occurrence suggest slumping as a formative mechanism of the disorganized bed. The differential diagenesis of the limestone conglomerate and sandstone beds contributes to their contrasting behavior, with the former exhibiting brittle deformation and the latter displaying ductile deformation. As a result, the rigid limestone conglomerate beds experienced brecciation, while the partially consolidated sandstone beds underwent soft-sediment deformation and filled the interstitial spaces.

Significantly, dendrolite bioherms and deformation structures within the limestone conglomerate bed are observed in the uppermost part of the lower section in the Sododong section. Correlating the Sododong section with the middle member of the Sesong Formation provides evidence of a non-depositional interval during the deposition of the middle member. Overall, the Sododong section yields valuable insights into the Sesong Formation, particularly with regard to the distinctive characteristics observed within the limestone conglomerate beds and dendrolite bioherms.

References

Allen, J. R. L., 1986. Earthquake magnitude-frequency, epicentral distance, and soft-sediment deformation in sedimentary basins. Sedimentary Geology, 46(1-2), 67-75.

Álvaro, J. J., Clausen, S., 2010. Morphology and ultrastructure of epilithic versus cryptic, microbial growth in lower Cambrian phosphorites from the Montagne Noire, France. Geobiology, 8(2), 89-100.

Anketell, J. M., Cegła, J., Dżułyński, S., 1970. On the deformational structures in systems with reversed density gradients. In Annales Societatis Geologorum Poloniae (Vol. 40, No. 1, pp. 3-30).

Aoti, K., 1942. Geology of Bunkei District in Tyosen with special references to the stratigraphy of the Tyosen Group. Journal of the Geological Society of Japan, 49, 279-281.

Bjerrum, L., 1973. Geotechnical problems involved in foundations of structures in the North Sea. Geotechnique, 23(3), 319-358.

Bradley, J. A., Daille, L. K., Trivedi, C. B., Bojanowski, C. L., Stamps, B. W., Stevenson, B. S., Nunn, H. S., Johnson, H. A., Loyd, S. J., Berelson, W. M., Corsetti, F. A., Spear, J. R., 2017. Carbonate-rich dendrolitic cones: Insights into a modern analog for incipient microbialite formation, Little Hot Creek, Long Valley Caldera, California. Npj Biofilms and Microbiomes, 3(1).

Braga, J. C., Martin, J. M., Wood, J. L., 2001. Submarine lobes and feeder channels of redeposited, temperate carbonate and mixed siliciclastic-carbonate platform deposits (Vera Basin, Almeria, southern Spain). Sedimentology, 48(1), 99-116.

Burne, R. V., Moore, L. S., 1987. Microbialites: organosedimentary deposits of benthic microbial communities. Palaios, 241-254.

Chen, J., Chough, S. K., Chun, S. S., Han, Z., 2009. Limestone pseudoconglomerates in the Late Cambrian Gushan and Chaomidian Formations (Shandong Province, China):

soft-sediment deformation induced by storm-wave loading. Sedimentology, 56(4), 1174-1195.

Chen, J., Chough, S. K., Han, Z., Lee, J. H., 2011. An extensive erosion surface of a strongly deformed limestone bed in the Gushan and Chaomidian formations (late Middle Cambrian to Furongian), Shandong Province, China: Sequence–stratigraphic implications. Sedimentary Geology, 233(1-4), 129-149.

Chen, J., Chough, S. K., Lee, J. H., Han, Z., 2012. Sequence-stratigraphic comparison of the upper Cambrian Series 3 to Furongian succession between the Shandong region, China and the Taebaek area, Korea: High variability of bounding surfaces in an epeiric platform. Geosciences Journal, 16(4), 357–379.

Chen, J., Han, Z., Zhang, X., Fan, A., Yang, R. 2010. Early diagenetic deformation structures of the Furongian ribbon rocks in Shandong Province of China—A new perspective of the genesis of limestone conglomerates. Science China Earth Sciences, 53(2), 241-252.

Chen, J., Lee, H. S., 2013. Soft-sediment deformation structures in Cambrian siliciclastic and carbonate storm deposits (Shandong Province, China): Differential liquefaction and fluidization triggered by storm-wave loading. Sedimentary Geology, 288, 81-94.

Chen, J., Lee, J. H., 2014. Current progress on the geological record of microbialites and microbial carbonates. Acta Geologica Sinica-English Edition, 88(1), 260-275.

Cheong, C. H. 1969. Stratigraphy and paleontology of the Samcheog coalfield, Gangweondo, Korea (I). Geological Society of Korea, 5(1), 13-55.

Cho, E., Hong, J., 2021. Cyclic patterns in the Lower Ordovician Dumugol Formation, Korea: Influence of compaction on sequence-stratigraphic interpretation in mixed carbonate–shale successions. Sedimentary Geology, 420, 105942.

Choi, D. K., 1998. The Yongwol Group (Cambrian-Ordovician) redefined: a proposal for the stratigraphic nomenclature of the Choson Supergroup. Geosciences Journal, 2(4),

220-234.

Choi, D.K., Chough, S.K., 2005. The Cambrian-Ordovician stratigraphy of the Taebaeksan Basin, Korea: a review. Geosciences Journal, 9(2), 187-214.

Choi, D. K., Chough, S. K., Kwon, Y. K., Lee, S. B., Woo, J., Kang, I., Lee, D. J., 2004. Taebaek group (Cambrian-Ordovician) in the Seokgaejae section, Taebaeksan Basin: a refined lower Paleozoic stratigraphy in Korea. Geosciences Journal, 8(2), 125-151.

Choi, D.K., Lee, J.G., Lee, S.B., Park, T.Y., Hong, P., 2016. Trilobite Biostratigraphy of the lower Paleozoic (Cambrian–Ordovician) Joseon Supergroup, Taebaeksan Basin, Korea. Acta Geologica Sinica-English Edition, 90(6), 1976-1999.

Chough, S. K., Kwon, S. T., Ree, J. H., Choi, D. K., 2000. Tectonic and sedimentary evolution of the Korean peninsula: a review and new view. Earth-Science Reviews, 52(1-3), 175-235.

Chough, S. K., Lee, H. S., Woo, J., Chen, J., Choi, D. K., Lee, S. B., Han, Z., 2010. Cambrian stratigraphy of the North China Platform: revisiting principal sections in Shandong Province, China. Geosciences Journal, 14(3), 235-268.

Collinson, J., Mountney, N., Thompson, D. (2006). Sedimentary Structures (3rd). In Terra, England (pp. 1-292).

Crevello, P. D., Schlager, W. (1980). Carbonate debris sheets and turbidites, Exuma Sound, Bahamas. Journal of Sedimentary Research, 50(4), 1121-1147.

Cumberpatch, Z. A., Soutter, E. L., Kane, I. A., Casson, M., Vincent, S. J. (2021). Evolution of a mixed siliciclastic-carbonate deep-marine system on an unstable margin: The Cretaceous of the Eastern Greater Caucasus, Azerbaijan. Basin Research, 33(1), 612-647.

Demicco, R. V., Hardie, L. A., 1994. Sedimentary structures and early diagenetic features of shallow marine carbonates. SEPM atlas series, 1, 265.

Dixon, J. F., Steel, R. J., Olariu, C., 2013. A model for cutting and healing of deltaic mouth

bars at the shelf edge: mechanism for basin-margin accretion. Journal of Sedimentary Research, 83(3), 284-299.

Drzewiecki, P. A., Simó, J. A., 2002. Depositional processes, triggering mechanisms and sediment composition of carbonate gravity flow deposits: examples from the Late Cretaceous of the south-central Pyrenees, Spain. Sedimentary Geology, 146(1-2), 155-189.

Duncan, M., 2007. Lateral variability in shallow marine ichnofabrics: implications for the ichnofabric analysis method. Journal of the Geological Society Vol. 164.

Droser, M. L., Bottjer, D. J., 1988. Trends in depth and extent of bioturbation in Cambrian carbonate marine environments, western United States. Geology, 16(3), 233-236.

Ferronatto, J. P. F., dos Santos Scherer, C. M., Drago, G. B., Rodrigues, A. G., de Souza, E. G., dos Reis, A. D., Cazarin, C. L., 2021. Mixed carbonate-siliciclastic sedimentation in a Mesoproterozoic storm-dominated ramp: Depositional processes and stromatolite development. Precambrian Research, 361, 106240.

Flügel, E., Munnecke, A., 2010. Microfacies of carbonate rocks: analysis, interpretation and application (Vol. 976, p. 2004). Berlin: springer.

Frey, R. W., Pemberton, S. G., Fagerstrom, J. A., 1984. Morphological, ethological, and environmental significance of the ichnogenera Scoyenia and Ancorichnus. Journal of Paleontology, 511-528.

Frey, R. W., Seilacher, A., 1980. Uniformity in marine invertebrate ichnology. Lethaia, 13(3), 183-207.

Galloway, W. E., Hobday, D. K., Galloway, W. E., Hobday, D. K. (1996). Terrigenous shelf systems. Terrigenous Clastic Depositional Systems: Applications to Fossil Fuel and Groundwater Resources, 159-185.

Glumac, B., Walker, K. R., 2002. Effects of grand-cycle cessation on the diagenesis of Upper Cambrian carbonate deposits in the southern Appalachians, USA. Journal of

Sedimentary Research, 72(4), 570-586.

Gong, Y. Y., 2016. Sedimentary fabrics for the Cambrian thrombolite bioherm: An example from the Zhangxia Formation in western Shandong Province. Geoscience, 30(2), 436-444.

Grey, K., Awramik, S. M., 2020. Handbook for the study and description of microbialites. Geological Survey of Western Australia.

Hiscott, R. N., James, N. P., 1985. Carbonate debris flows, Cow Head Group, western Newfoundland. Journal of Sedimentary Research, 55(5), 735-745.

Howell, J., Woo, J., Chough, S. K., 2011. Dendroid morphology and growth patterns: 3-D computed tomographic reconstruction. Palaeogeography, Palaeoclimatology, Palaeoecology, 299(1-2), 335-347.

James, N. P., Dalrymple, R. W., 2010. Facies Models 4, Geotext. Geol. Associ. Canada, Memor. Univ. Newfoundland, St. Johns.

Jeyapalan, J. K., Duncan, J. M., Seed, H. B., 1983. Investigation of flow failures of tailings dams. Journal of geotechnical engineering, 109(2), 172-189.

Jinmin, S., Ping, L., Shisheng, Y., Di, Y., Chuanmin, Z., Pengwei, L., Xiufen, Z., 2014. Reservoirs of Lower Cambrian microbial carbonates, Tarim Basin, NW China. Petroleum Exploration and Development, 41(4), 449-459.

Joo, H., Ryu, I.C., 2012. Sedimentary facies of the Cambrian Sesong Formation, Taebacksan Basin. In Econ. Environ. Geol (Vol. 45, Issue 5).

Kim, Y. H. G., Woo, J., Park, T. Y. S., Kihm, J. H., Lee, J. I., Choe, M. Y., 2018. Sedimentary breccia and diamictite of the Cambrian Spurs Formation in northern Victoria Land, Antarctica: two kinds of debris flows in a submarine channel system. Antarctic Science, 30(4), 245-263.

Kobayashi, T., 1966, The Cambro-Ordovician formations and faunas of South Korea, Part X, Stratigraphy of the Chosen Group in Korea and South Manchuria and its relation to

the Cambro-Ordovician formations and faunas of other areas, Section A, The Chosen Group of South Korea.

Kreisa, R. D., 1981. Storm-generated sedimentary structures in subtidal marine facies with examples from the Middle and Upper Ordovician of southwestern Virginia. Journal of Sedimentary Research, 51(3), 823-848.

Kruse, P. D., Zhuravlev, A. Y., 2008. Middle–Late Cambrian Rankenella–Girvanella reefs of the Mila Formation, northern Iran. canadian Journal of Earth sciences, 45(6), 619-639.

Kwon, Y., 2012. Sequence Stratigraphy of the Yeongweol Group (Cambrian-Ordovician), Taebaeksan Basin, Korea: Paleogeographic Implications. Econ. Environ. Geol Vol. 45, Issue 3.

Kwon, Y. K., Chough, S. K., Choi, D. K., Lee, D. J., 2002. Origin of limestone conglomerates in the Choson Supergroup (Cambro–Ordovician), mid-east Korea. Sedimentary Geology, 146(3-4), 265-283.

Kwon, Y. K., Chough, S. K., Choi, D. K., Lee, D. J., 2006. Sequence stratigraphy of the Taebaek Group (Cambrian-Ordovician), Mideast Korea. Sedimentary Geology, 192(1–2), 19–55.

Lee, B. S., 2014. Conodonts from the Sesong Slate and Hwajeol Formation (Guzhangian to Furongian) in the Taebaeksan Basin, Korea. Acta Geologica Sinica-English Edition, 88(1), 35-45.

Lee, H. S., Chough, S. K., 2011. Depositional processes of the Zhushadong and Mantou formations (Early to Middle Cambrian), Shandong Province, China: roles of archipelago and mixed carbonate–siliciclastic sedimentation on cycle genesis during initial flooding of the North China Platform. Sedimentology, 58(6), 1530-1572.

Lee, J. H., Chen, J., Chough, S. K., 2015. The middle-late Cambrian reef transition and related geological events: A review and new view. In Earth-Science Reviews (Vol. 145, pp. 66–84). Elsevier.

Lee, J. H., Cho, S. H., Jung, D. Y., Choh, S. J., Lee, D. J., 2021. Ribbon rocks revisited: the upper Cambrian (Furongian) Hwajeol Formation, Taebaek Group, Korea. Facies, 67(3), 19.

Lee, Jeong-Hyun., Hong, Jongsun., Woo, Jusun., Oh, Jae-Ryong., Lee, Dong-Jin., Choh, Suk-Joo., 2016. Reefs in the early Paleozoic Taebaek Group, Korea: a review. Acta Geologica Sinica-English Edition, 90(1), 352-367.

Lee, J. H., Kim, B. J., Liang, K., Park, T. Y., Choh, S. J., Lee, D. J., Woo, J., 2016. Cambrian reefs in the western north China platform, Wuhai, inner Mongolia. Acta Geologica Sinica-English Edition, 90(6), 1946-1954.

Li, W., Chen, J., Hakim, A. J., Myrow, P. M., 2022. Middle Ordovician mass-transport deposits from western Inner Mongolia, China: Mechanisms and implications for basin evolution. Sedimentology, 69(3), 1301-1338.

Li, Y., Craven, J., Schweig, E. S., Obermeier, S. F., 1996. Sand boils induced by the 1993 Mississippi River flood: Could they one day be misinterpreted as earthquake-induced liquefaction?. Geology, 24(2), 171-174.

Lim, J. N., Chung, G. S., Park, T.-Y. S., Lee, K. S., 2015. Lithofacies and Stable Carbon Isotope Stratigraphy of the Cambrian Sesong Formation in the Taebaeksan Basin, Korea. Journal of the Korean Earth Science Society, 36(7), 617–631.

Luternauer, J. L., Finn, W. L., 1983. Stability of the Fraser River delta front. Canadian Geotechnical Journal, 20(4), 603-616.

MacEachern, J. A., Pemberton, S. G., Gingras, M. K., Bann, K. L., Dafoe, L. T., 2007. Uses of trace fossils in genetic stratigraphy. In Trace fossils (pp. 110-134). Elsevier.

Macquaker, J. H. S., Gawthorpe, R. L., 1993. Mudstone lithofacies in the Kimmeridge Clay Formation, Wessex Basin, southern England; implications for the origin and controls of the distribution of mudstones. Journal of Sedimentary Research, 63(6), 1129-1143.

Martinez, J.F., Cartwright, J., Hall, B., 2005. 3D seismic interpretation of slump complexes: examples from the continental margin of Israel. Basin Research, 17(1), pp.83-108.

Mei, M. X., Riaz, M., Zhang, Z. W., Meng, Q. F., Hu, Y., 2021. Diversified calcimicrobes in dendrolites of the Zhangxia Formation, Miaolingian Series (Middle Cambrian) of the North China craton. Journal of Palaeogeography, 10, 1-25.

Munson, P. J., Ann Munson, C., Pond, E. C. (1995). Paleoliquefaction evidence for a strong Holocene earthquake in south-central Indiana. Geology, 23(4), 325-328.

Myrow, P. M., Tice, L., Archuleta, B., Clark, B., Taylor, J. F., Ripperdan, R. L., 2004. Flat-pebble conglomerate: its multiple origins and relationship to metre-scale depositional cycles. Sedimentology, 51(5), 973-996.

Nataraja, M. S., Gill, H. S., 1983. Ocean wave-induced liquefaction analysis. Journal of Geotechnical Engineering, 109(4), 573-590.

Obermeier, S. F., 1996. Use of liquefaction-induced features for paleoseismic analysis—an overview of how seismic liquefaction features can be distinguished from other features and how their regional distribution and properties of source sediment can be used to infer the location and strength of Holocene paleo-earthquakes. Engineering Geology, 44(1-4), 1-76.

Oliveira, C. M., Hodgson, D. M., Flint, S. S., 2011. Distribution of soft-sediment deformation structures in clinoform successions of the Permian Ecca Group, Karoo Basin, South Africa. Sedimentary Geology, 235(3-4), 314-330.

Owen, G., Moretti, M., 2011. Identifying triggers for liquefaction-induced soft-sediment

deformation in sands. Sedimentary Geology, 235(3-4), 141-147.

Owen, G., Moretti, M., Alfaro, P., 2011. Recognising triggers for soft-sediment deformation: current understanding and future directions. Sedimentary Geology, 235(3-4), 133-140.

Park, T. Y. Choi, D. K., 2012. Middle Furongian (Late Cambrian) Shumardiids from the Sesong Formation, Taebaek Group, Korea. Journal of Paleontology, 86(1), 51-59.

Pattison, S. A., 1995. Sequence stratigraphic significance of sharp-based lowstand shoreface deposits, Kenilworth Member, Book Cliffs, Utah. AAPG bulletin, 79(3), 444-462.

Pemberton, S. G., 1992. Applications of ichnology to petroleum exploration (Vol. 17, pp. 141-167). SEPM Society for Sedimentary Geology.

Price, N. J., Cosgrove, J. W., 1990. Analysis of geological structures. Cambridge University Press.

Pujalte, V., Robador, A., Payros, A., Samsó, J. M., 2016. A siliciclastic braid delta within a lower Paleogene carbonate platform (Ordesa-Monte Perdido National Park, southern Pyrenees, Spain): record of the Paleocene–Eocene thermal maximum perturbation. Palaeogeography, palaeoclimatology, palaeoecology, 459, 453-470.

Riding, R., 1991. Classification of microbial carbonates. Calcareous algae and stromatolites, 2, 1-51.

Riding, R., 2000. Microbial carbonates: the geological record of calcified bacterial–algal mats and biofilms. Sedimentology, 47, 179-214.

Riding, R., 2002. Structure and composition of organic reefs and carbonate mud mounds: concepts and categories. Earth-Science Reviews, 58(1-2), 163-231.

Riding, R., 2011. Microbialites, stromatolites, and thrombolites. In Encyclopedia of geobiology.

Rowland, S. M., Shapiro, R. S., 2002. Reef patterns and environmental influences in the

Cambrian and earliest Ordovician.

Saltzman, M. R., Cowan, C. A., Runkel, A. C., Runnegar, B., Stewart, M. C., Palmer, A. R., 2004. The Late Cambrian SPICE (δ13C) event and the Sauk II-Sauk III regression: new evidence from Laurentian basins in Utah, Iowa, and Newfoundland. Journal of Sedimentary Research, 74(3), 366-377.

Seed, H. B., 1979. Soil liquefaction and cyclic mobility evaluation for level ground during earthquakes. Journal of the geotechnical engineering division, 105(2), 201-255.

Seibel, B. A., Drazen, J. C., 2007. The rate of metabolism in marine animals: environmental constraints, ecological demands and energetic opportunities. Philosophical Transactions of the Royal Society B: Biological Sciences, 362(1487), 2061-2078.

Seilacher, A., 2007. Trace fossil analysis. Springer Science & Business Media.

Seilacher, A., Buatois, L. A., Mángano, M. G., 2005. Trace fossils in the Ediacaran–Cambrian transition: behavioral diversification, ecological turnover and environmental shift. Palaeogeography, Palaeoclimatology, Palaeoecology, 227(4), 323-356.

Shanmugam, G., 2010. Slides, slumps, debris flow, and turbidity currents. Ocean Currents: A Derivative of the Encyclopedia of Ocean Sciences, 20, 418.

Shapiro, R. S., 1998. Upper Cambrian-lowermost Ordovician stratigraphy and microbialites of the Great Basin, United States. University of California, Santa Barbara.

Shapiro, R. S., Awramik, S. M., 2000. Microbialite morphostratigraphy as a tool for correlating Late Cambrian–Early Ordovician sequences. The Journal of Geology, 108(2), 171-180.

Shapiro, R. S., Rigby, J. K., 2004. First occurrence of an in situ anthaspidellid sponge in a dendrolite mound (Upper Cambrian; Great Basin, USA). Journal of Paleontology, 78(4), 645-650.

Stanley Jr, G. D. (Ed.)., 2001. The history and sedimentology of ancient reef systems (Vol. 17). Springer Science Business Media.

Suosaari, E. P., Awramik, S. M., Reid, R. P., Stolz, J. F., Grey, K., 2018. Living dendrolitic microbial mats in Hamelin pool, Shark Bay, Western Australia. Geosciences, 8(6), 212.

Taylor, A. M., Goldring, R., 1993. Description and analysis of bioturbation and ichnofabric. Journal of the Geological Society, 150(1), 141-148.

Tucker, M. E., 2003. Sedimentary rocks in the field. John Wiley & Sons.

Tucker, M. E., 2011. Sedimentary rocks in the field: a practical guide. John Wiley & Sons.

Tucker, M. E., Wright, V. P., 2009. Carbonate sedimentology. John Wiley & Sons.

Van Houten, F. B., Bhattacharyya, D. P., 1982. Phanerozoic oolitic ironstones--Geologic record and facies model. Annual Review of Earth and Planetary Sciences, 10(1), 441-457.

Vieira, F. V., Bastos, A. C., Quaresma, V. S., Leite, M. D., Costa Jr, A., Oliveira, K. S., Amado Filho, G. M., 2019. Along-shelf changes in mixed carbonate-siliciclastic sedimentation patterns. Continental Shelf Research, 187, 103964.

Walter, A., Colacicchi, R., Mantanari, A., 1985. Synsedimentary slides and bedding formation in Apennine pelagic limestones. Journal of Sedimentary Research, 55(5), 720-734.

Watts, P., Grilli, S. T., Tappin, D. R., Fryer, G. J., 2005. Tsunami generation by submarine mass failure. II: Predictive equations and case studies. Journal of waterway, port, coastal, and ocean engineering, 131(6), 298-310.

Wilson, J. L., 2012. Carbonate facies in geologic history. Springer Science Business Media.

Woo, J., Chough, S. K., 2010. Growth patterns of the Cambrian microbialite: phototropism and speciation of Epiphyton. Sedimentary Geology, 229(1-2), 1-8.

Woo, J., Chough, S. K., Han, Z., 2008. Chambers of Epiphyton thalli in microbial

buildups, Zhangxia formation (Middle Cambrian), Shandong province, China. Palaios, 23(1), 55-64.

Woo, J., Kim, Y. H. S., Chough, S. K., 2019. Facies and platform development of a microbe-dominated carbonate platform: The Zhangxia Formation (Drumian, Cambrian Series 3), Shandong Province, China. Geological Journal, 54(4), 1993-2015.

Zamora, S., Clausen, S., Álvaro, J. J., Smith, A. B., 2010. Pelmatozoan echinoderms as colonizers of carbonate firmgrounds in mid-Cambrian high energy environments. Palaios, 25(12), 764-768.

Zeller, M., Verwer, K., Eberli, G. P., Massaferro, J. L., Schwarz, E., Spalletti, L., 2015. Depositional controls on mixed carbonate–siliciclastic cycles and sequences on gently inclined shelf profiles. Sedimentology, 62(7), 2009-2037.

Zhuravlev, A. Y., 1996. Reef ecosystem recovery after the Early Cambrian extinction. Geological Society, London, Special Publications, 102(1), 79-96.

Appendix

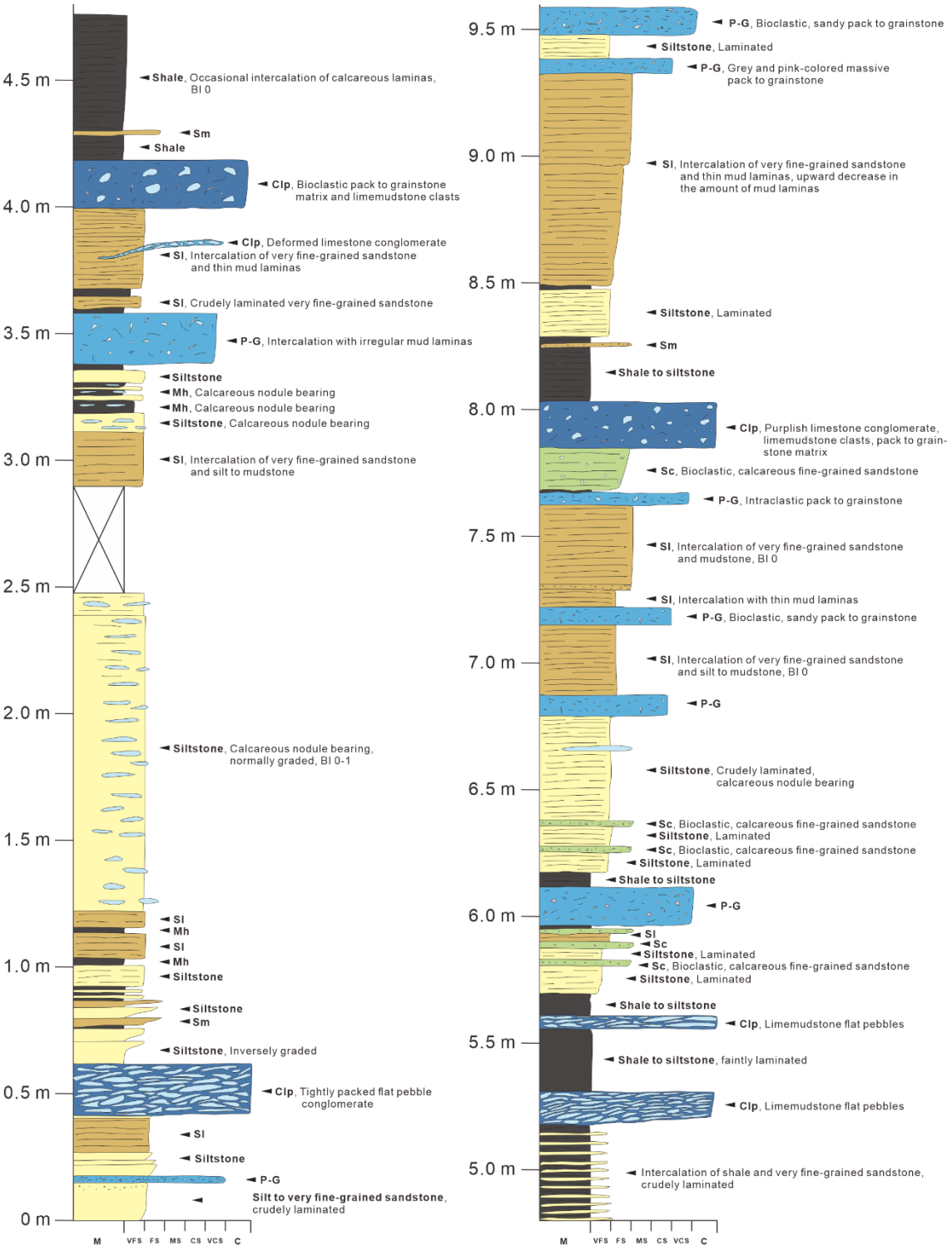
4.5 m
4.0 m
3.5 m
3.0 m
2.5 m
2.0 m
1.5 m
1.0 m
0.5 m
0 m
Shale, Occasional intercalation of calcareous laminas, BI 0
Sm
Shale
Clp, Bioclastic pack to grainstone matrix and limemudstone clasts
Clp, Deformed limestone conglomerate
Sl, Intercalation of very fine-grained sandstone and thin mud laminas
Sl, Crudely laminated very fine-grained sandstone
P-G, Intercalation with irregular mud laminas
Siltstone
Mh, Calcareous nodule bearing
Mh, Calcareous nodule bearing
Siltstone, Calcareous nodule bearing
Sl, Intercalation of very fine-grained sandstone and silt to mudstone
Siltstone, Calcareous nodule bearing, normally graded, BI 0-1
Sl
Mh
Sl
Mh
Siltstone
Siltstone
Sm
Siltstone, Inversely graded
Clp, Tightly packed flat pebble conglomerate
Sl
Siltstone
P-G
Silt to very fine-grained sandstone, crudely laminated
M
VFS FS MS CS VCS C
9.5 m
9.0 m
8.5 m
8.0 m
7.5 m
7.0 m
6.5 m
6.0 m
5.5 m
5.0 m
P-G, Bioclastic, sandy pack to grainstone
Siltstone, Laminated
P-G, Grey and pink-colored massive pack to grainstone
Sl, Intercalation of very fine-grained sandstone and thin mud laminas, upward decrease in the amount of mud laminas
Siltstone, Laminated
Sm
Shale to siltstone
Clp, Purplish limestone conglomerate, limemudstone clasts, pack to grainstone matrix
Sc, Bioclastic, calcareous fine-grained sandstone
P-G, Intraclastic pack to grainstone
Sl, Intercalation of very fine-grained sandstone and mudstone, BI 0
Sl, Intercalation with thin mud laminas
P-G, Bioclastic, sandy pack to grainstone
Sl, Intercalation of very fine-grained sandstone and silt to mudstone, BI 0
P-G
Siltstone, Crudely laminated, calcareous nodule bearing
Sc, Bioclastic, calcareous fine-grained sandstone
Siltstone, Laminated
Sc, Bioclastic, calcareous fine-grained sandstone
Siltstone, Laminated
Shale to siltstone
P-G
Sl
Sc
Siltstone, Laminated
Sc, Bioclastic, calcareous fine-grained sandstone
Siltstone, Laminated
Shale to siltstone
Clp, Limemudstone flat pebbles
Shale to siltstone, faintly laminated
Clp, Limemudstone flat pebbles
Intercalation of shale and very fine-grained sandstone, crudely laminated
M
VFS FS MS CS VCS C

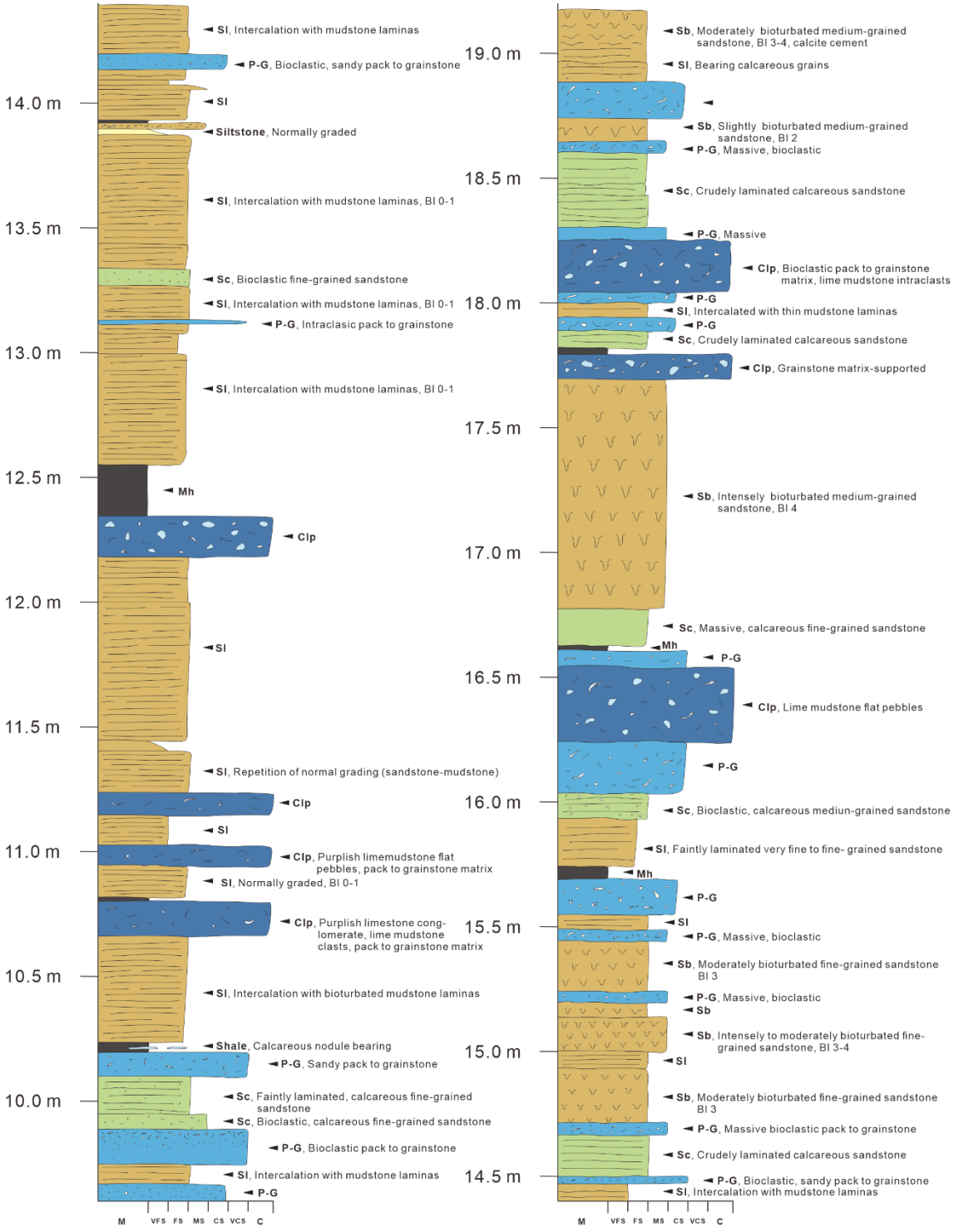
14.0 m
13.5 m
13.0 m
12.5 m
12.0 m
11.5 m
11.0 m
10.5 m
10.0 m
Sl, Intercalation with mudstone laminas
P-G, Bioclastic, sandy pack to grainstone
Sl
Siltstone, Normally graded
Sl, Intercalation with mudstone laminas, Bl 0-1
Sc, Bioclastic fine-grained sandstone
Sl, Intercalation with mudstone laminas, Bl 0-1
P-G, Intraclasic pack to grainstone
Sl, Intercalation with mudstone laminas, Bl 0-1
Mh
Clp
Sl
Sl, Repetition of normal grading (sandstone-mudstone)
Clp
Sl
Clp, Purplish limemudstone flat pebbles, pack to grainstone matrix
Sl, Normally graded, Bl 0-1
Clp, Purplish limestone conglomerate, lime mudstone clasts, pack to grainstone matrix
Sl, Intercalation with bioturbated mudstone laminas
Shale, Calcareous nodule bearing
P-G, Sandy pack to grainstone
Sc, Faintly laminated, calcareous fine-grained sandstone
Sc, Bioclastic, calcareous fine-grained sandstone
P-G, Bioclastic pack to grainstone
Sl, Intercalation with mudstone laminas
P-G
M
VFS
FS
MS
CS
VCS
C
19.0 m
18.5 m
18.0 m
17.5 m
17.0 m
16.5 m
16.0 m
15.5 m
15.0 m
14.5 m
Sb, Moderately bioturbated medium-grained sandstone, Bl 3-4, calcite cement
Sl, Bearing calcareous grains
Sb, Slightly bioturbated medium-grained sandstone, Bl 2
P-G, Massive, bioclastic
Sc, Crudely laminated calcareous sandstone
P-G, Massive
Clp, Bioclastic pack to grainstone matrix, lime mudstone intraclasts
P-G
Sl, Intercalated with thin mudstone laminas
P-G
Sc, Crudely laminated calcareous sandstone
Clp, Grainstone matrix-supported
Sb, Intensely bioturbated medium-grained sandstone, Bl 4
Sc, Massive, calcareous fine-grained sandstone
Mh
P-G
Clp, Lime mudstone flat pebbles
P-G
Sc, Bioclastic, calcareous mediun-grained sandstone
Sl, Faintly laminated very fine to fine- grained sandstone
Mh
P-G
Sl
P-G, Massive, bioclastic
Sb, Moderately bioturbated fine-grained sandstone Bl 3
P-G, Massive, bioclastic
Sb
Sb, Intensely to moderately bioturbated fine-grained sandstone, Bl 3-4
Sl
Sb, Moderately bioturbated fine-grained sandstone Bl 3
P-G, Massive bioclastic pack to grainstone
Sc, Crudely laminated calcareous sandstone
P-G, Bioclastic, sandy pack to grainstone
Sl, Intercalation with mudstone laminas
M
VFS
FS
MS
CS
VCS
C

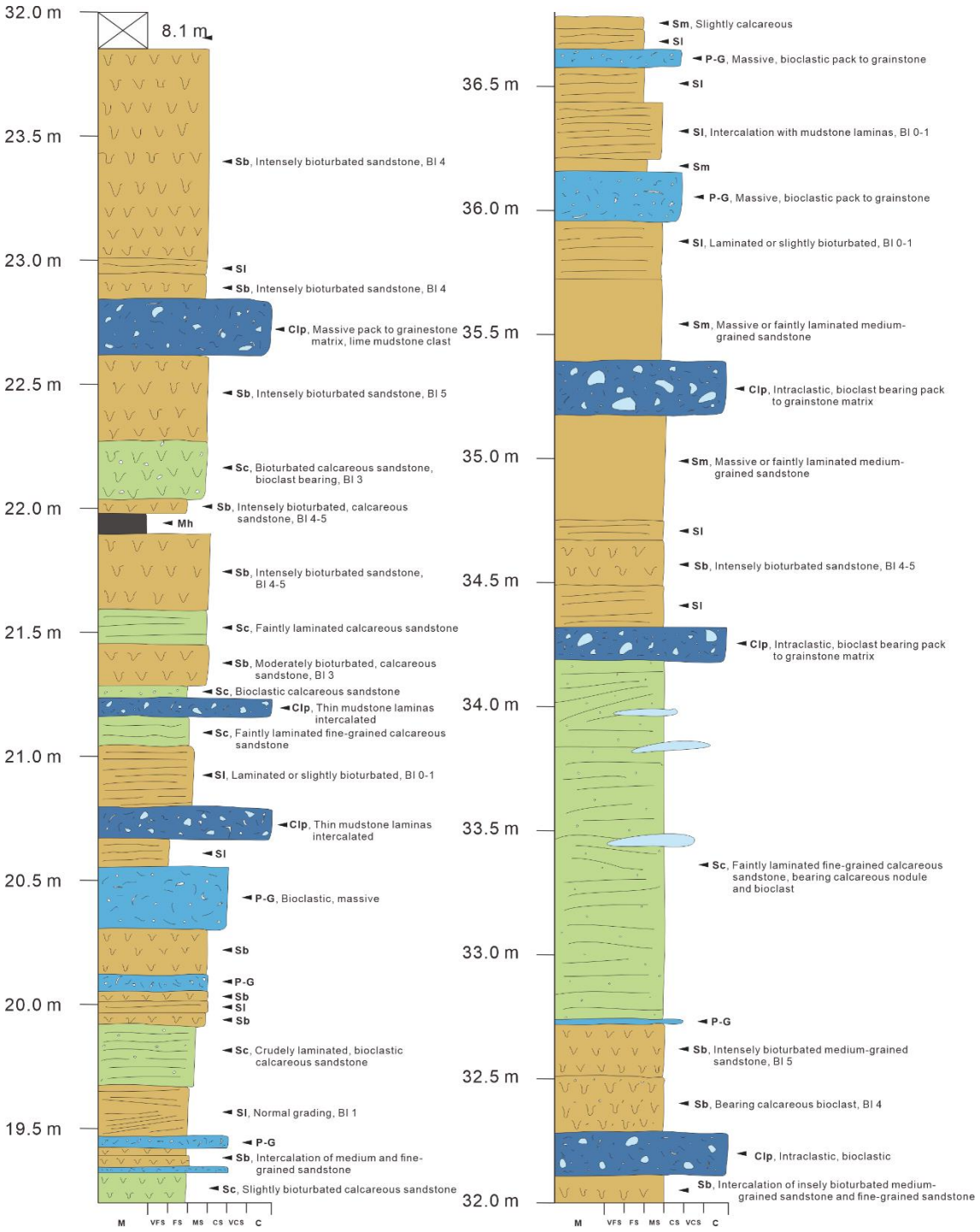
32.0 m
8.1 m
23.5 m
Sb, Intensely bioturbated sandstone, BI 4
23.0 m
Sl
Sb, Intensely bioturbated sandstone, BI 4
Clp, Massive pack to grainestone matrix, lime mudstone clast
22.5 m
Sb, Intensely bioturbated sandstone, BI 5
Sc, Bioturbated calcareous sandstone, bioclast bearing, BI 3
22.0 m
Sb, Intensely bioturbated, calcareous sandstone, BI 4-5
Mh
Sb, Intensely bioturbated sandstone, BI 4-5
21.5 m
Sc, Faintly laminated calcareous sandstone
Sb, Moderately bioturbated, calcareous sandstone, BI 3
Sc, Bioclastic calcareous sandstone
Clp, Thin mudstone laminas intercalated
Sc, Faintly laminated fine-grained calcareous sandstone
21.0 m
Sl, Laminated or slightly bioturbated, BI 0-1
Clp, Thin mudstone laminas intercalated
Sl
20.5 m
P-G, Bioclastic, massive
Sb
P-G
20.0 m
Sb
Sl
Sb
Sc, Crudely laminated, bioclastic calcareous sandstone
Sl, Normal grading, BI 1
19.5 m
P-G
Sb, Intercalation of medium and fine-grained sandstone
Sc, Slightly bioturbated calcareous sandstone
M VFS FS MS CS VCS C
Sm, Slightly calcareous
Sl
P-G, Massive, bioclastic pack to grainstone
36.5 m
Sl
Sl, Intercalation with mudstone laminas, BI 0-1
Sm
36.0 m
P-G, Massive, bioclastic pack to grainstone
Sl, Laminated or slightly bioturbated, BI 0-1
Sm, Massive or faintly laminated medium-grained sandstone
35.5 m
Clp, Intraclastic, bioclast bearing pack to grainstone matrix
35.0 m
Sm, Massive or faintly laminated medium-grained sandstone
Sl
Sb, Intensely bioturbated sandstone, BI 4-5
34.5 m
Sl
Clp, Intraclastic, bioclast bearing pack to grainstone matrix
34.0 m
33.5 m
Sc, Faintly laminated fine-grained calcareous sandstone, bearing calcareous nodule and bioclast
33.0 m
P-G
Sb, Intensely bioturbated medium-grained sandstone, BI 5
32.5 m
Sb, Bearing calcareous bioclast, BI 4
Clp, Intraclastic, bioclastic
Sb, Intercalation of insely bioturbated medium-grained sandstone and fine-grained sandstone
32.0 m
M VFS FS MS CS VCS C

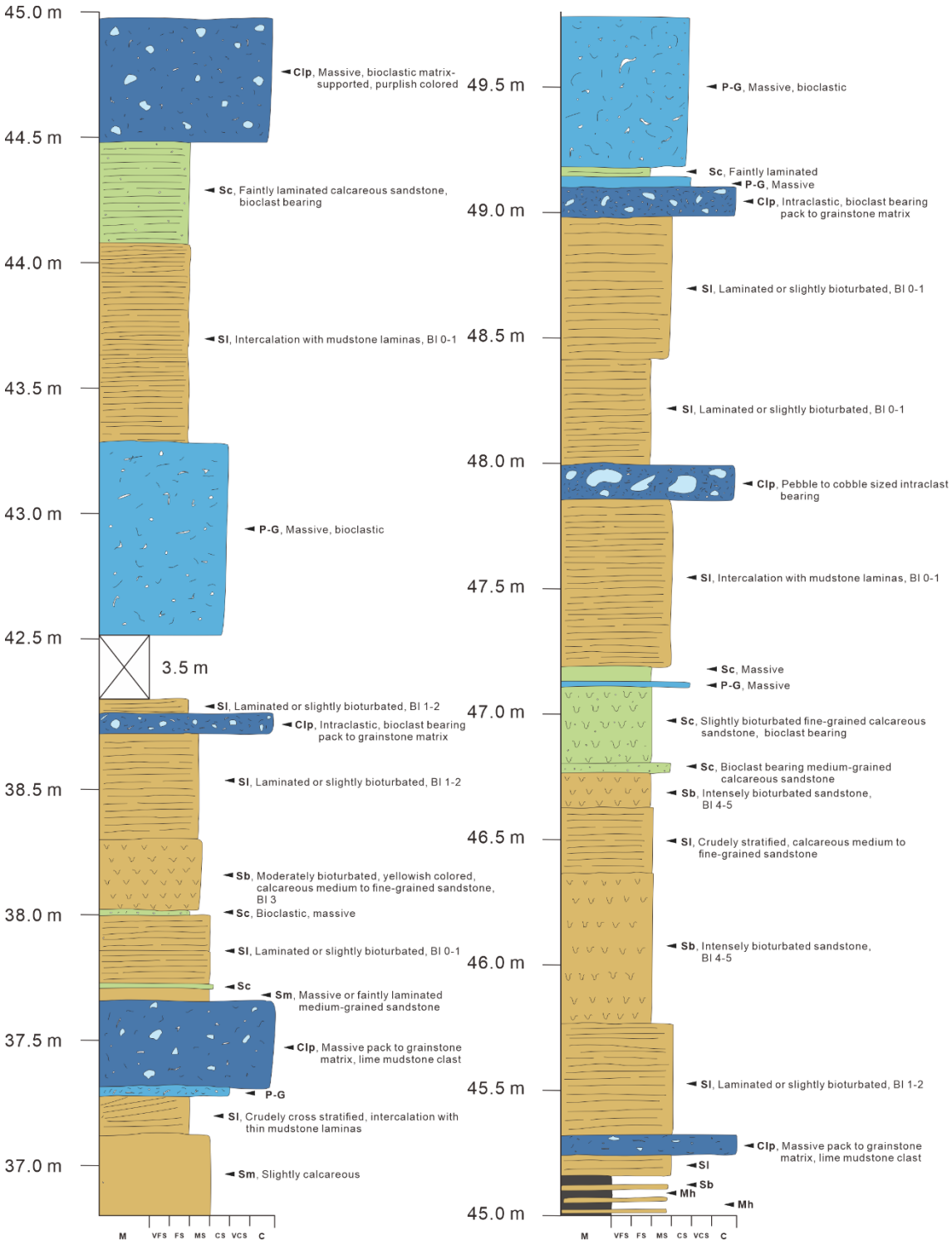
45.0 m
44.5 m
44.0 m
43.5 m
43.0 m
42.5 m
38.5 m
38.0 m
37.5 m
37.0 m
Clp, Massive, bioclastic matrix-supported, purplish colored
Sc, Faintly laminated calcareous sandstone, bioclast bearing
Sl, Intercalation with mudstone laminas, Bl 0-1
P-G, Massive, bioclastic
3.5 m
Sl, Laminated or slightly bioturbated, Bl 1-2
Clp, Intraclastic, bioclast bearing pack to grainstone matrix
Sl, Laminated or slightly bioturbated, Bl 1-2
Sb, Moderately bioturbated, yellowish colored, calcareous medium to fine-grained sandstone, Bl 3
Sc, Bioclastic, massive
Sl, Laminated or slightly bioturbated, Bl 0-1
Sc
Sm, Massive or faintly laminated medium-grained sandstone
Clp, Massive pack to grainstone matrix, lime mudstone clast
P-G
Sl, Crudely cross stratified, intercalation with thin mudstone laminas
Sm, Slightly calcareous
M VFS FS MS CS VCS C
49.5 m
49.0 m
48.5 m
48.0 m
47.5 m
47.0 m
46.5 m
46.0 m
45.5 m
45.0 m
P-G, Massive, bioclastic
Sc, Faintly laminated
P-G, Massive
Clp, Intraclastic, bioclast bearing pack to grainstone matrix
Sl, Laminated or slightly bioturbated, Bl 0-1
Sl, Laminated or slightly bioturbated, Bl 0-1
Clp, Pebble to cobble sized intraclast bearing
Sl, Intercalation with mudstone laminas, Bl 0-1
Sc, Massive
P-G, Massive
Sc, Slightly bioturbated fine-grained calcareous sandstone, bioclast bearing
Sc, Bioclast bearing medium-grained calcareous sandstone
Sb, Intensely bioturbated sandstone, Bl 4-5
Sl, Crudely stratified, calcareous medium to fine-grained sandstone
Sb, Intensely bioturbated sandstone, Bl 4-5
Sl, Laminated or slightly bioturbated, Bl 1-2
Clp, Massive pack to grainstone matrix, lime mudstone clast
Sl
Sb
Mh
Mh
M VFS FS MS CS VCS C

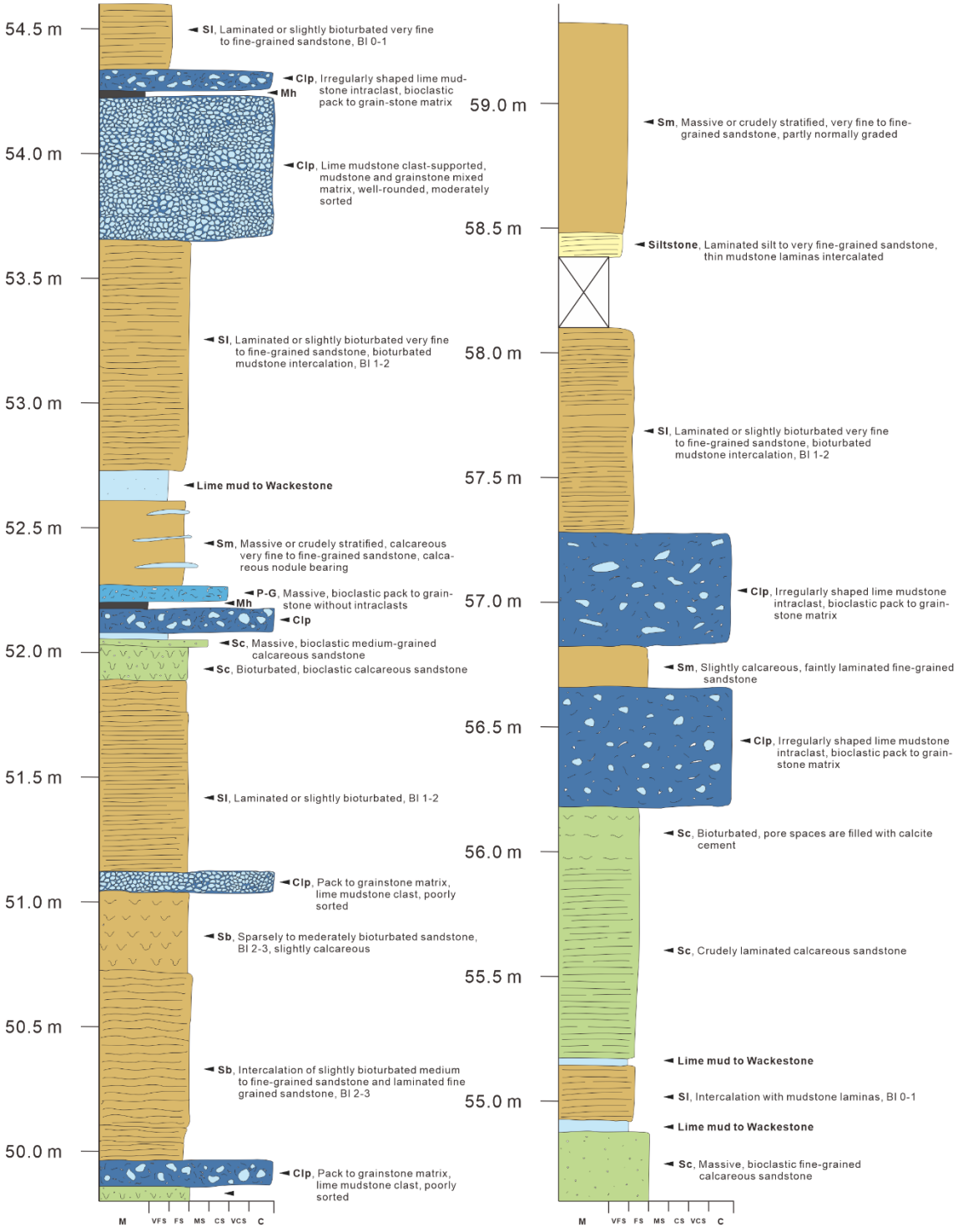
54.5 m
54.0 m
53.5 m
53.0 m
52.5 m
52.0 m
51.5 m
51.0 m
50.5 m
50.0 m
59.0 m
58.5 m
58.0 m
57.5 m
57.0 m
56.5 m
56.0 m
55.5 m
55.0 m
Sl, Laminated or slightly bioturbated very fine to fine-grained sandstone, BI 0-1
Clp, Irregularly shaped lime mudstone intraclast, bioclastic pack to grain-stone matrix
Mh
Clp, Lime mudstone clast-supported, mudstone and grainstone mixed matrix, well-rounded, moderately sorted
Sl, Laminated or slightly bioturbated very fine to fine-grained sandstone, bioturbated mudstone intercalation, BI 1-2
Lime mud to Wackestone
Sm, Massive or crudely stratified, calcareous very fine to fine-grained sandstone, calcareous nodule bearing
P-G, Massive, bioclastic pack to grain-stone without intraclasts
Mh
Clp
Sc, Massive, bioclastic medium-grained calcareous sandstone
Sc, Bioturbated, bioclastic calcareous sandstone
Sl, Laminated or slightly bioturbated, BI 1-2
Clp, Pack to grainstone matrix, lime mudstone clast, poorly sorted
Sb, Sparsely to mederately bioturbated sandstone, BI 2-3, slightly calcareous
Sb, Intercalation of slightly bioturbated medium to fine-grained sandstone and laminated fine grained sandstone, BI 2-3
Clp, Pack to grainstone matrix, lime mudstone clast, poorly sorted
M VFS FS MS CS VCS C
Sm, Massive or crudely stratified, very fine to fine-grained sandstone, partly normally graded
Siltstone, Laminated silt to very fine-grained sandstone, thin mudstone laminas intercalated
Sl, Laminated or slightly bioturbated very fine to fine-grained sandstone, bioturbated mudstone intercalation, BI 1-2
Clp, Irregularly shaped lime mudstone intraclast, bioclastic pack to grain-stone matrix
Sm, Slightly calcareous, faintly laminated fine-grained sandstone
Clp, Irregularly shaped lime mudstone intraclast, bioclastic pack to grain-stone matrix
Sc, Bioturbated, pore spaces are filled with calcite cement
Sc, Crudely laminated calcareous sandstone
Lime mud to Wackestone
Sl, Intercalation with mudstone laminas, BI 0-1
Lime mud to Wackestone
Sc, Massive, bioclastic fine-grained calcareous sandstone
M VFS FS MS CS VCS C

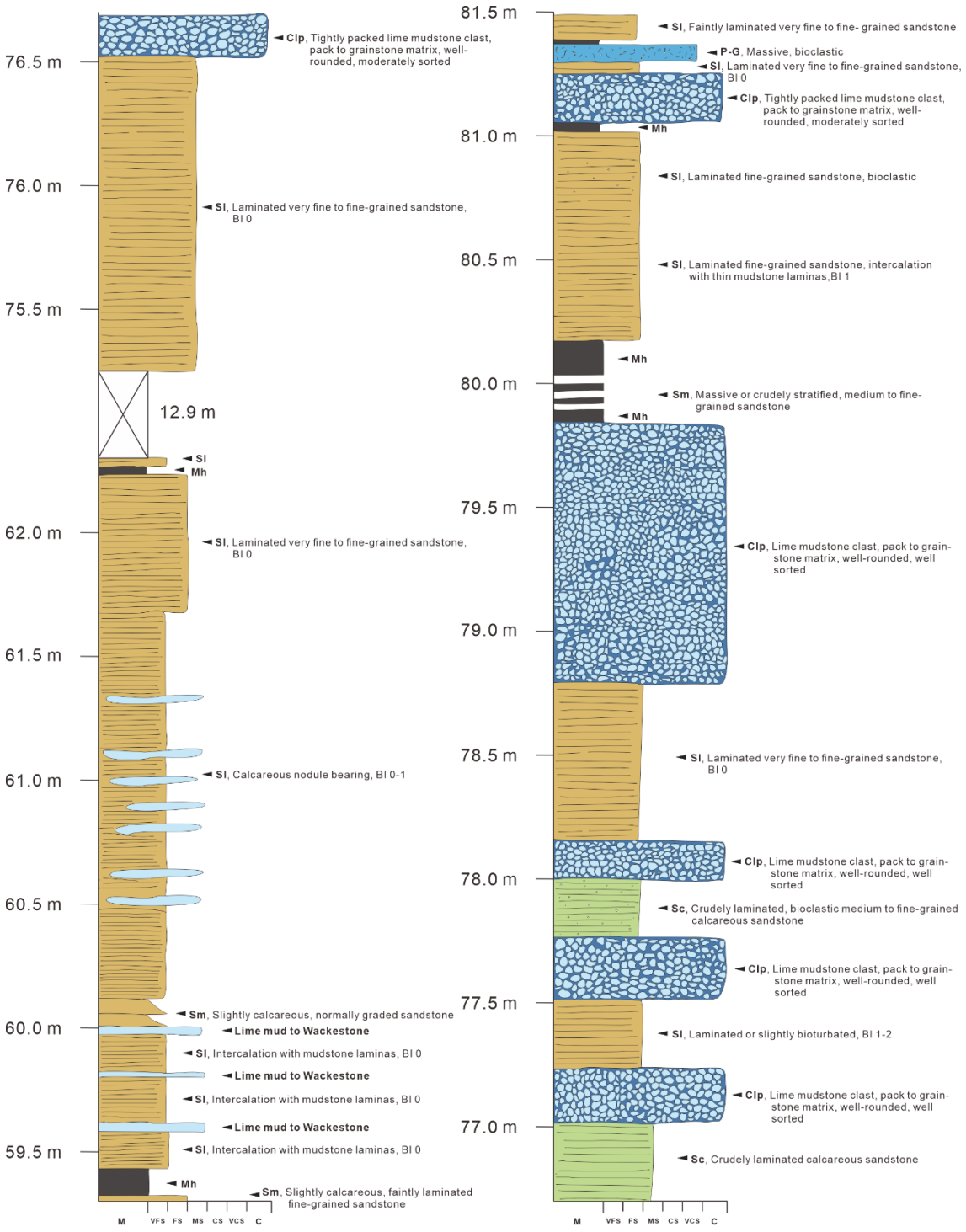
76.5 m
76.0 m
75.5 m
62.0 m
61.5 m
61.0 m
60.5 m
60.0 m
59.5 m
12.9 m
Clp, Tightly packed lime mudstone clast, pack to grainstone matrix, well-rounded, moderately sorted
Sl, Laminated very fine to fine-grained sandstone, Bl 0
Sl
Mh
Sl, Laminated very fine to fine-grained sandstone, Bl 0
Sl, Calcareous nodule bearing, Bl 0-1
Sm, Slightly calcareous, normally graded sandstone
Lime mud to Wackestone
Sl, Intercalation with mudstone laminas, Bl 0
Lime mud to Wackestone
Sl, Intercalation with mudstone laminas, Bl 0
Lime mud to Wackestone
Sl, Intercalation with mudstone laminas, Bl 0
Mh
Sm, Slightly calcareous, faintly laminated fine-grained sandstone
M VFS FS MS CS VCS C
81.5 m
81.0 m
80.5 m
80.0 m
79.5 m
79.0 m
78.5 m
78.0 m
77.5 m
77.0 m
Sl, Faintly laminated very fine to fine- grained sandstone
P-G, Massive, bioclastic
Sl, Laminated very fine to fine-grained sandstone, Bl 0
Clp, Tightly packed lime mudstone clast, pack to grainstone matrix, well-rounded, moderately sorted
Mh
Sl, Laminated fine-grained sandstone, bioclastic
Sl, Laminated fine-grained sandstone, intercalation with thin mudstone laminas,Bl 1
Mh
Sm, Massive or crudely stratified, medium to fine-grained sandstone
Mh
Clp, Lime mudstone clast, pack to grain-stone matrix, well-rounded, well sorted
Sl, Laminated very fine to fine-grained sandstone, Bl 0
Clp, Lime mudstone clast, pack to grain-stone matrix, well-rounded, well sorted
Sc, Crudely laminated, bioclastic medium to fine-grained calcareous sandstone
Clp, Lime mudstone clast, pack to grain-stone matrix, well-rounded, well sorted
Sl, Laminated or slightly bioturbated, Bl 1-2
Clp, Lime mudstone clast, pack to grain-stone matrix, well-rounded, well sorted
Sc, Crudely laminated calcareous sandstone
M VFS FS MS CS VCS C

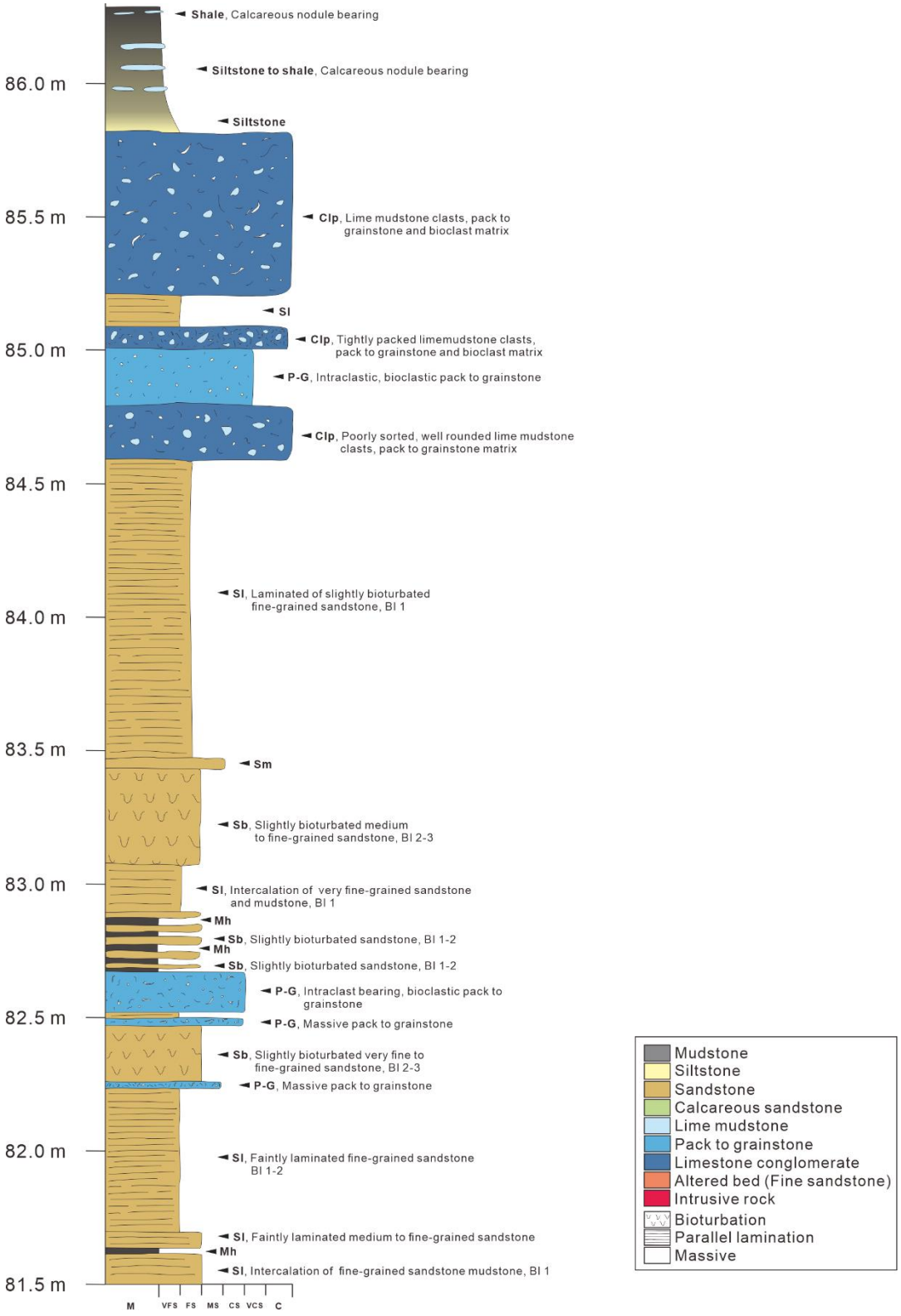
86.0 m
85.5 m
85.0 m
84.5 m
84.0 m
83.5 m
83.0 m
82.5 m
82.0 m
81.5 m
Shale, Calcareous nodule bearing
Siltstone to shale, Calcareous nodule bearing
Siltstone
Clp, Lime mudstone clasts, pack to grainstone and bioclast matrix
Sl
Clp, Tightly packed limemudstone clasts, pack to grainstone and bioclast matrix
P-G, Intraclastic, bioclastic pack to grainstone
Clp, Poorly sorted, well rounded lime mudstone clasts, pack to grainstone matrix
Sl, Laminated of slightly bioturbated fine-grained sandstone, Bl 1
Sm
Sb, Slightly bioturbated medium to fine-grained sandstone, Bl 2-3
Sl, Intercalation of very fine-grained sandstone and mudstone, Bl 1
Mh
Sb, Slightly bioturbated sandstone, Bl 1-2
Mh
Sb, Slightly bioturbated sandstone, Bl 1-2
P-G, Intraclast bearing, bioclastic pack to grainstone
P-G, Massive pack to grainstone
Sb, Slightly bioturbated very fine to fine-grained sandstone, Bl 2-3
P-G, Massive pack to grainstone
Sl, Faintly laminated fine-grained sandstone Bl 1-2
Sl, Faintly laminated medium to fine-grained sandstone
Mh
Sl, Intercalation of fine-grained sandstone mudstone, Bl 1
M
VFS
FS
MS
CS
VCS
C
Mudstone
Siltstone
Sandstone
Calcareous sandstone
Lime mudstone
Pack to grainstone
Limestone conglomerate
Altered bed (Fine sandstone)
Intrusive rock
Bioturbation
Parallel lamination
Massive

요약(국문초록)

이 연구에서는 태백산분지 내 태백지역의 세송층 상부 사암체의 시추코어와 야외노두를 통해 세송층에 대한 정밀퇴적상 분석을 진행했다. 세송층은 주된 암상에 따라 세일로 구성되는 하부와 사암으로 구성되는 상부로 나뉜다. 이 중 기저부를 제외한 사암구간은 총 여덟 개의 퇴적상으로 구성되어 있다. 퇴적상과 생교란작용 강도 정보의 조합으로 세송층 사암의 퇴적상조합을 세 개로 구분할 수 있었고, 각 퇴적상조합이 지시하는 퇴적환경을 해석하였다. 각 퇴적상조합은 해안전면부와 외해 사이의 외해 전이대 환경에서 퇴적되었다. 퇴적상조합 1은 주로 강한 생교란작용을 받은 중립질 사암으로 이루어져 있으며 해안전면부 환경과 가장 가까운 환경으로 해석된다. 퇴적상조합 2는 입도와 생교란작용의 강도가 감소하는 경향이 보이며 퇴적상조합 3은 생교란작용이 거의 없이 가장 세립한 입자들로 구성된다는 점에서 외해 방향에 가까워지고 수심이 깊어지는 퇴적환경을 지시한다. 이러한 퇴적환경의 변화는 세송층의 퇴적이 상대해수면 변화에 의해 조절되었음을 지시한다. 추가적으로 세송층에서 독특한 변형구조를 가지는 석회역암과 그 위에서 자라난 덴드롤라이트의 형성 및 변형 과정을 상세히 기술하였다. 세송층에서 발견된 적이 없는 변형구조는 사면에서의 슬럼프에 의한 제한된 횡적이동으로 해석되었다. 이는 일반적인 램프형태의 탄산염 대지보다 큰 사면이 세송층의 퇴적 당시에 존재하였을 수 있음을 지시한다. 또한 여러 단면으로 연장되지 않는 하드그라운드 등 지역적인 퇴적률 변화를 지시하는 구조는 횡적으로 변화가 심한 퇴적시스템을 암시한다. 이와

같은 증거는 탄산염대지에 규산염 쇄설성 퇴적물을 공급하는 삼각주가 존재할 수 있는 가능성을 보여준다. 이러한 변형구조 및 덴드롤라이트 건층을 이용하여 북중국 대륙 및 동시대 다른 지역과 대비하여 세송층 퇴적환경 변화를 유발한 요인을 이해하는데 기여할 수 있을 것으로 기대한다.

주요어 : 퇴적상분석, 퇴적환경, 외해 전이대, 슬럼핑, 미생물암, 후기 캠브리아기

학번 : 2021-28244